GENERATING CELLS FOR LUNG TISSUE ENGINEERING

A THESIS SUBMITTED TO THE FACULTY OF THE GRADUATE SCHOOL OF THE UNIVERSITY OF MINNESOTA BY

Aylin Turgut

IN PARTIAL FULFILLMENT OF THE REQUIREMENTS FOR THE DEGREE OF MASTER OF SCIENCE

Dr. Angela Panoskaltsis-Mortari

May 2014

Acknowledgements

I would like thank Andy Price, Carolyn Meyer and Mona Schmidt in our laboratory for their technical assistance with my work. I would also like to thank Dr. Meri Firpo for her assistance with the stirred flask bioreactor setup.

Abstract

Decellularization of essential organs such as the lung has become an integral part of regenerative medicine. As the availability of donors is very low reseeding of these decellularized organs with a patient's own cells is a potential therapy for those desperately in need. This way, the risks associated with allogeneic immune rejection are avoided. Some research groups have been successful in reseeding the lung with allogeneic differentiated cells. However, the barrier to presently overcome is to seed with stem cells and ensure these cells differentiate to all the desired cell types of the lung. Another obstacle is obtaining the desired number of cells for recellularization of large organs such as the lung. Scale-up methods using stirred vessel bioreactors with conditions similar to the physiological environment are a desirable alternative to conventional cell culture. In this study, I demonstrate large-scale cell culture in stirred flask bioreactors by facing the challenges of scale-up from 2D to 3D suspension culture. I also show the existence of exosomes in decellularized pig and mouse lung and identify the miRNAs (miRNAs) contained within them. MicroRNAs are becoming increasingly popular research tools as they are known to regulate many essential processes. Exosomes are enriched with miRNAs and can be shuttled between cells, thereby affecting target cell behavior. I utilized the exosomes from decellularized lungs in directed differentiation of induced pluripotent stem cells (iPSCs) to the definitive endoderm (DE) lineage and compared it with conventional differentiation methods. The exosomes had a profound effect on the morphology of the cells which will lead to further studies on exosome-directed differentiation procedures.

Table of Contents

List of Tables

List of Figures

List of Abbreviations

AEC: alveolar epithelial cell

bFGF: basal fibroblast growth factor

BM: bone marrow

BSA: bovine serum albumin

COPD: chronic obstructive pulmonary disease

DC: dendritic cell

DE: definitive endoderm

DEPC: diethylpyrocarbonate

DI: de-ionized

EC: electrode cleaner

ECM: extracellular matrix

EDTA: Ethylenediaminetetraacetic acid

EP: endodermal progenitor

ESC: embryonic stem cell

GAPDH: glyceraldehyde-3-phosphate dehydrogenase

HPC:hematopoietic progenitor cell

iPSC: induced pluripotent stem cell

miRNA: microRNA

MM: multiple myeloma cell

MSC: mesenchymal stromal cell

MVB: multivesicular body

NaCl: sodium chloride

OD: optical density

PBS: phosphate-buffered saline

qRT-PCR: real-time reverse transcription polymerase chain reaction

ROCK: Rho-associated protein kinase

RQI: RNA quality index

Introduction

Lung tissue engineering is one of the least studied tissue engineering fields. The lung is a very large, complex organ with many cell types that have various functions. The demand for lungs is high and the waiting list for lung transplants is long. Therefore, there is an urgent need for the engineered organ. One way to potentially regenerate large organs is to decellularize them, leaving the extracellular matrix with the correct structure and molecular cues still present. The aim is to inject autologous induced pluripotent stem cells (iPSCs) or lung progenitors into the matrix so that the cells will be able to proliferate and differentiate in the right environment. iPSCs are differentiated cells that are reprogrammed to pluripotent stem cells which have the capability to differentiate into all cell types (Takahashi et al., 2007). Their applications are vast and I hypothesized that when iPSCs or iPSC-derived definitive endoderm (DE) cells are injected into the decellularized lung, they would give rise to the desired cell types. However, a huge number of these cells are required to regenerate a mouse lung (likely millions) and a pig lung (likely billions). Generating this number on 2D culture plates is time-consuming and inefficient, as a large number of plates would be required. Stirred flask bioreactors are large vessels that can carry large volumes of media. They can be set up so that conditions such as oxygen and carbon dioxide levels, the shear stress the cells experience, humidity and temperature in the flask resemble the physiological conditions of the human body. Many studies have demonstrated the scale-up of 2D cell cultures to 3D suspension cultures (Abbasalizadeh et al. 2012, Amit et al., 2011). The largest barrier to overcome is the change in environment the cells experience when they are moved from cell culture plates, where they normally adhere to the bottom of the plate, to suspension in stirred

flask bioreactors. In these studies, 3D suspension culture conditions were made similar to 2D culture and media changes were done more frequently, to ensure the cells received enough nutrients to expand in a large vessel. Additional factors that help cell growth in suspension to compensate for the loss of an adherent surface have been used in suspension culture studies (Chen et al., Horani et al., 2007). In this study by Chen et al, the ROCK (Rho-associated protein kinase) inhibitor was tried to facilitate cell culture scale-up. This molecule is known to inhibit apoptosis associated with cell dissociation in suspension culture (Watanabe et al., 2007). In addition, the use of serum-free culture media eliminates the uncertainty of sourcing associated with animal products (Ozturk and Hu, 2006). 3D stem cell suspension cultures are currently maintained in chemically-defined media which allow for precise identification of media components so that the most suitable media can be chosen for the appropriate type of cell culture (Ozturk and Hu, 2006). Scale-up of definitive endoderm culture would be highly desirable prior to lung recellularization as endodermal progenitor cells (EPs) are closer to mature lung cells down the differentiation pathway. Therefore, they might be able to differentiate and reconstitute the decellularized lung matrix more easily than iPSCs. The first step prior to large-scale cell culture would be to obtain endodermal progenitor cells. IPSC differentiation to definitive endoderm has been successful using specific small molecule, namely growth factors (Cheng et al., 2012). The main growth factors that drive differentiation are Activin and Wnt3a and are added in a precisely timed manner during cell culture.

The extracellular matrix (ECM) plays a crucial role in providing the right environment for cell growth, adhesion, proliferation and differentiation. It is not only a physical

scaffold for the cells but also induces biochemical and biomechanical signals that organize the cells within it (Frantz et al., 2010). This is aided by structural molecules of the ECM such as collagen, elastin, laminin and fibronectin which enable the cells to adhere in the correct places in a timely manner. A large component of the ECM is proteoglycans which can bind growth factors that are secreted by the cells. This establishes a growth gradient for the cells during development (Hynes et al. 2009). In addition, the ECM itself contains molecules that induce vessel formation, cell migration or attachment (Hynes et al., 2009). The ECM is organ and tissue-specific so it is a very heterogenous structure (Frantz et al. 2010). The bronchi, for example, have an ECM with a very different composition and structure compared to the ECM of the distal part of the lung that contains the alveoli. The decellularized lung matrix could provide the correct 3D structure and molecular cues to direct development of the injected iPSCs or iPSC-derived DE. Cells injected into synthetic 3D matrices such as poly(lactide) acid (PLA), poly (glycolide) acid (PGA) and polyethylene glycol adhere well and interact with the synthetic substrate (Villa-Diaz et al., 2013). 3D matrices have the advantage that they resemble the physiological state of the living organism compared to 2D cultures. Therefore, observations made in 3D culture or matrices will be more relevant as the cells reside in an environment strongly resembling their own. Cell growth and viability can be improved with the use of bioreactors especially when a large initial cell population is used. 3D culture also can improve cell differentiation to definitive endoderm shown by increased expression of DE markers and higher cell viability compared to 2D cultures (Hoveizi et al., 2013). Many small molecules govern the fate of stem cells during development. Normal mammalian development of the lungs begins by the formation of a

bud from the primitive foregut and this finely tuned process gives rise to around 40 different cell types which derive from the endoderm (Krauss-Etschmann et al., 2013). The pulmonary vessels and smooth muscle of the airway arise from the mesoderm. The expression of the right signaling molecules at a precise time is essential for normal lung development. Disruption of this process leads to abnormal pulmonary phenotypes (Rock et al. 2012). Perhaps one of the most important regulatory molecules during development is microRNAs (miRNAs). They can bind complementary mRNA sequences and suppress their expression after transcription. This way, they can regulate cell proliferation, differentiation and programmed cell death (Ekstrom et al., 2007). It is known that miRNAs are contained in small vesicles inside the cell called exosomes and can be transported from one cell to another, thereby controlling the fates of different target tissues (Storvoogel et al. and Andaloussi et al., 2012).

Exosomes originate from multivesicular bodies (MVBs) in the cell, which are formed by the fusion of late endosomes (Stoorvogel et al., 2012). This gives rise to a larger compartment surrounded by a lipid membrane containing many vesicles. These MVBs can then fuse with the plasma membrane and the vesicles are exocytosed to the extracellular environment. The contents of each exosome depend on the cell type they are released from and the conditions under which they are released. Exosomes contain small RNAs, mainly microRNAs and some rRNAs which are delivered to the extracellular environment or target cells if the exosomes fuse with other cell membranes. Many biological fluids such as blood, serum, saliva and breast milk contain exosomes, as well as cells. Exosomes have been implicated to work as vehicles for miRNA and mRNA delivery from one cell to another (Stoorvogel et al., 2012). The mRNA is then translated

to protein in the target cell, which can affect cell function (Valadi et al., 2007). Since the miRNAs in exosomes can vary depending on the tissue in which they reside in, the presence of these miRNAs have been used for tissue identification. (Liang et al., 2007).

The miRNAs in the exosomes of neurodegenerate brain tissue differ from normal tissue. Exosomes are synthesized in a distinct manner in the cell, involving the plasma membrane, trans-Golgi network and lysosomes. The inward budding of these compartments relative to the cytosol form MVBs containing the vesicles. It was found that proteins such as amyloid precursor protein and prions are associated with exosomes and are transported from one cell type to another by exploiting this pathway. There has been growing evidence for the exploitation of this pathway in Parkinson's disease progression. The misfolded α-synuclein protein is thought to be transmitted from neuron to neuron in exosomes, thereby spreading the misfolded protein to healthy cells. This eventually leads to apoptosis of dopaminergic neuronal cells and ultimately disease progression towards reduction of the substantia nigra part of the brain (Russo et al. 2012).

Initial studies of exosomes have shown they have a role in the immune system, for example, in dendritic cells (DCs) (Stoorvogel et al., 2012). Depending on the activation status of the host dendritic cell, the miRNAs in immature DCs can differ greatly from the miRNAs in mature, activated DCs indicating a miRNA signature for these exosomes.

Studies on multiple myeloma (MM) cells showed that bone marrow mesenchymal stromal cell (MSC) exosomes carry unique miRNAs that can be transferred to clonal multiple myeloma plasma cells which causes cell proliferation and dissemination, thereby enhancing tumor progression. (Roccaro et al., 2013) The same study also demonstrated

that exosomes from MM BM (bone marrow)-MSCs carried potentially oncogenic proteins that affect MM cell migration and adhesion in the bone marrow microenvironment.

The miRNA can also act as oncogenes or tumor suppressors. Recent studies have shown that miR506 can selectively kill late-stage lung cancer cells when ectopically expressed (Yin et al., 2014). The molecule is normally used as a marker for lung cancer progression since its expression increases toward the end-stage of the disease. When synthetic mimics of miR506 were injected into lung cancer cells and normal cells, the former were killed whereas the latter were not affected. This is quite similar to the concept of how p53 becomes oncogenic when it is normally a tumor suppressor. Therefore, when ectopically expressed, molecules such as p53 and miR506, will kill cancer tissue and not their normal counterparts as their normal functions are to regulate signaling networks in the cell. miR506 downregulates NF-κB to decrease cell proliferation and activate p53. Therefore, it is postulated that the lung cancer cells have infinite NF-κB signaling and this makes the cancer cells more dependent on NF-κB as the cancer progresses. Hence, when miR506 is ectopically expressed, late-stage lung cancer cells were the most severely affected. Findings like this support the important roles of miRNAs in life-threatening diseases and how they can potentially be used as therapeutic molecules for other fatal lung diseases such as cystic fibrosis, idiopathic pulmonary fibrosis and chronic obstructive pulmonary disease (COPD) (Sessa et al., 2013)

Similar to the concept of cancer cells versus normal cells, exosomal miRNAs in undifferentiated progenitor cells also differ from mature, differentiated cells. These

features of exosomes may facilitate the delivery of therapeutic molecules to cancerous tissue and help identification of the differentiation stage of a particular cell in tissue engineering approaches. In a recent study, miRNA expression profiling showed that iPSCs and fibroblasts had distinct miRNA signatures (Porciuncula et al. 2013). Activin A is a molecule used for differentiation of iPSCs or ESCs to definitive endoderm. Activin-induced iPSCs have certain miRNAs, including miR17, upregulated compared to untreated iPSCs. This provides evidence that the cells have a miRNA signature unique to each stage of cell differentiation. MiR375 is another miRNA known to be highly upregulated in definitive endoderm and is highly conserved across species (Hinton et al 2010).

Perhaps the most popular tissue engineering approach at present is decellularization of the desired organ with various detergents, leaving the extracellular matrix of the organ. It is postulated that this decellularized matrix will provide the right niches and microenvironment for growth of cells that are injected into the decellularized organ. All tissues contain exosomes and their miRNA and protein content vary greatly depending on the tissue they originate from so we hypothesized that they may remain in pig and mouse lungs after decellularization. Assuming the exosomes are present in decellularized lung, their miRNA content can be identified and used to determine whether they induce differentiation or self-renewal. This way, the desired exosomes can be used as tools during the delivery of the iPSCs, endoderm progenitors, endothelial cells and other lung relevant cells to direct the differentiation process to the many various tissues of the lung. The exosomes would be co-cultured with the cells on plates before injection into the decellularized lung. Furthermore, current decellularization protocols of pig and human

lungs involve the use of detergents, de-ionised (DI) water, sodium chloride (NaCl), phosphate-buffered saline (PBS) and DNases (Price et al., 2010). This study demonstrated the absence of any genomic DNA that may have remained in the pig and human lungs after decellularization. A similar study showed this in decellularized pig and mouse lungs (Nichols et al, 2013) and in a nonhuman primate model (Bonvillain et al., 2012). Almost complete recellularization of the pig, mouse and human lungs with pulmonary cell types was successfully demonstrated by cell adherence to the acellular lung matrices. Cell attachment in the nonhuman primate model was shown with mesenchymal stromal cells (Bonvillain et al., 2012). However, it would be useful to know if anything remaining in the lung after decellularization could affect or be used as a tool in the regeneration process. The detergents are expected to wash out small particles such as exosomes because these vesicles have a phospholipid membrane that can bind the detergent molecules. However, as the exosomes may get lodged in certain parts of the lung such as the distal region, it is possible they may remain after decellularization. More importantly, RNases are not used to wash out the lung and exosomes mainly contain RNA and protein. This leads to the possibility that exosomes and their contents are preserved, even after decellularization.

In order for exosomes to be identified, they have to be analyzed for their RNA and protein content. They can be also observed under the electron microscope from a more macrobiological perspective. However, this is not enough as they are very small vesicles

and not every vesicle can be classified as an exosome. Therefore, their molecular content needs to be studied.

The miRNA relevant to the lung are miR15a, miR29b, miR29c and miR375. miR29b and miR29c are mainly expressed in adult pig and mouse lung (Sessa et al., 2013) and miR375 expression is highest in definitive endoderm cells (Li et al., 2014). The function of miR15a is unknown but is implicated to have a role in cell cycle regulation (Bandi et al., 2009). Therefore, it is possible these miRNAs remain in the decellularized mouse and pig lungs.

Overall, the aim of this study was to find a suitable scale-up method to generate sufficient numbers of iPSCs and iPSC-derived DE to reconstitute a decellularized lung. The specific scale-up method involved 3D culture of iPSCs in a stirred flask bioreactor. In addition to this, the existence of exosomes in the decellularized lung was explored to identify miRNAs that could possibly be used as tools for directing the development of desired cell types in the lung. If found, the exosomes would be co-cultured with iPSCs on 2D plates to observe any changes in cell phenotype and that way, their potential use in the recellularization process would be determined.

Materials and Methods

Bioreactor

iPS cells re-programmed from human skin fibroblasts (Stem Cell Institute, University of Minnesota, Minneapolis, Minnesota) were harvested from 6-well plates that were coated with Geltrex (ThermoFisher Scientific Inc, Grand Island, NY) (Figure 1). These cells were then placed in a Corning 125ml stirred flask bioreactor at a seeding density of 750,000 cells per ml in a sterile hood. Rho-associated protein kinase (ROCK) inhibitor was added at a 10μM working concentration. Therefore, 1μl of this 10μM solution was added as a 1 hour pre-treatment after cell dissocation using 0.5 mM EDTA (Invitrogen 15575-020 0.5 M EDTA, Invitrogen™, Carlsbad, California) to resuspend the cells and pipet them out of the 6-well plates. The cell suspension volume was 5ml so 70ml of mTESR™1 medium (Stemcell™Technologies, Vancouver, British Columbia, Canada) was added to give a total volume of 75ml (Figure 1). The medium was changed every 2 days by taking up 35ml medium and replacing it with 35ml of fresh medium. The conditions for cell culture were 37˚C, 5%CO_2, 4%O_2 and pH 7. A pan of water was kept in the incubator in order to keep the environment humid, thus preventing the cell cultures from drying out.

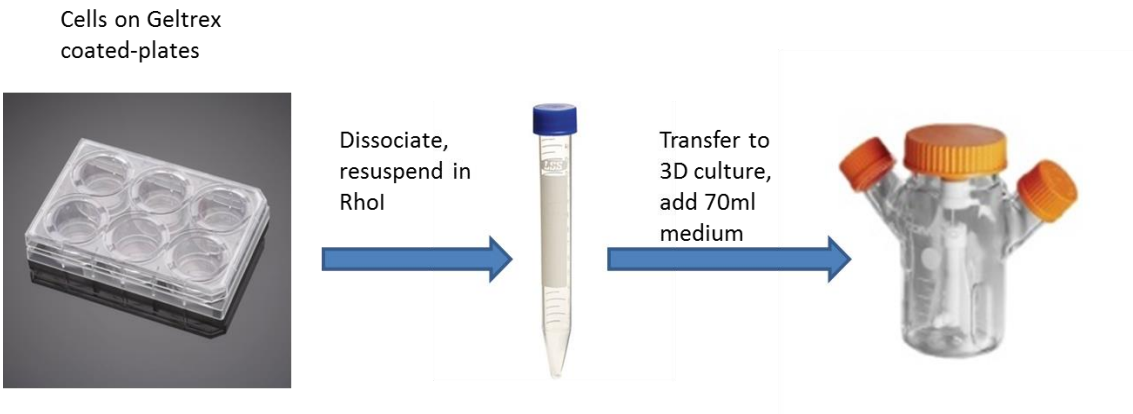

Figure 1: Schematic of bioreactor setup

Cell count using Trypan Blue Stain

Trypan Blue passively diffuses through the cell membrane once the cell has undergone apoptosis. 10µl of cell suspension was taken from the bioreactor cell culture and mixed with 10µl of Trypan Blue stain (Sigma-Aldrich, St. Louis, Missouri). The average numbers of total and dead cells were calculated from four counts in a hemocytometer.

5ml samples of cell suspension were taken every other day and centrifuged for five minutes at 1400rpm. The supernatant was taken for metabolite analysis and the cell suspension for RNA isolation.

Glucose Assay

The metabolites analyzed were glucose and lactate. Glucose levels in cell cultures were analyzed using a glucose assay kit (Sigma-Aldrich®, St. Louis, Missouri). The process essentially involved the oxidation of glucose to gluconic acid and peroxidase by the

enzyme glucose oxidase. The peroxidase, which is the enzyme, reacts with o-dianisidine reagent, the probe, which is colorless in reduced form. The result is a brown solution of o-dianisidine which is unstable. Sulfuric acid is added at the end of the experiment after a thirty minute incubation which causes the solution to turn into a range of pink colors. The absorbance of these colors at 540nm in a spectrophotometer is proportional to the glucose concentration of the sample and this is determined from a set of standards of 0.02, 0.04, 0.06 and 0.08mg of glucose per ml plotted on a curve. The samples need to be tested at several different dilutions to accurately determine the glucose concentration. 1:10, 1:100 and 1:1000 dilutions were tested for bioreactor samples of days 0, 2 and 4. The day 0 sample was supernatant from the cells which had been grown on 6-well plates. The 1:10 dilutions produced absorbance values too high to read off the standard curve and the 1:1000 dilutions produced absorbances that were too low. The 1:100 dilutions produced absorbance values within the range of the standard curve and therefore the glucose assay was repeated using only this dilution.

Lactate Assay

The lactate assay was performed using the lactate assay kit (Sigma-Aldrich®, St. Louis, Missouri). Firstly, the probe and lactate dehydrogenase enzyme were warmed to room temperature before use, protected from light. The lactate dehydrogenase enzyme was reconstituted in 220µl of lactate assay buffer. 10µl of the lactate standard provided in the kit was combined with 990µl of lactate assay buffer to generate a 1nmol/µl standard solution. The concentrations were obtained by plotting absorbances of samples against known concentrations of the lactate standard generated. These were added to a 96-well

plate. Lactate assay buffer was added to each well bring the volume to 50µl. 2µl each of enzyme mix and probe were added to the wells for the standards. Then, 2, 4, 6, 8 and 10µl of sample were added to the wells and the volume brought up to 50µl with lactate assay buffer. The various dilutions of all the samples were taken into account so that when the standard curve was generated, the values that fell in the linear part of the curve could be selected for data interpretation. The plate was read at 570nm using a spectrophotometer (Implen nanophotometer® P330).

Isolation of RNA

RNA was isolated using the phenol/chloroform extraction method with Trizol reagent as per Invitrogen RNA Isolation with Trizol protocol. The RNA was then purified using the Invitrogen RNA purification kit. The RNA concentrations and purities were measured using a spectrophotometer (Implen nanophotometer® P330). The spectrophotometer was set to RNA measurement. The cuvette and lids were cleaned with 75% ethanol. 1µl of DI water was pipetted onto the cuvette and used as a blank. The cuvette was cleaned with 75% ethanol and then 1µl of sample was pipetted onto the cuvette. The RNA concentration and A260/280 readings were recorded. An A260/A280 ratio of at least 2.0 indicates good RNA purity.

Conversion of RNA to cDNA

RNA was converted to cDNA using the SuperScript® III first-strand synthesis for qRT-PCR (Invitrogen™, Carlsbad, California). Prior to that, RNA samples were normalized

to the lowest concentration by dilution with nuclease-free water. Briefly, a master mix was prepared with 10µl of RT reaction mix, 2µl of RT enzyme mix, up to 1µg of RNA and up to 20µl of diethylpyrocarbonate(DEPC)-treated water. Water pre-treated with DEPC is used since this chemical inactivates the RNase enzymes present in the water so that there is no RNA degradation. The mixture was incubated at room temperature for 10 minutes. Then it was placed in the heat block and incubated at 50ºC for 30 minutes. The reaction was terminated at 85ºC at 5 minutes and then placed on ice. 1µl of E.Coli RNAase H was added to the samples and incubated at 37ºC for 20 minutes. The samples were then ready for PCR amplification.

Amplification of cDNA and agarose gel electrophoresis

The cDNA was amplified by reverse transcriptase-polymerase chain reaction (RT-PCR) using primers for mouse or human β-actin genes, depending on the sample origin. The master mix was prepared using 16.25 µl H_2O, 2.5 µl 10X salt buffer, 0.1 µl dNTP, 0.15 µl Taq, 2.5 µl of forward and 2.5 µl reverse primers and 1µl of cDNA sample. These values were multiplied by the number of samples required for cDNA amplification.

The forward and reverse primers for mouse and human cDNA were diluted tenfold. 2µl of primer and 18µl of water were put into each of the tubes. Then 2.5 µl of this mixture was added to the master mix (which is referred to above).

The PCR-amplified cDNA was then run on a 1% agarose gel (1% weight/volume in Tris-Acetate-EDTA buffer) and visualized with ethidium bromide.

Lung harvest and tissue homogenization

Normal and decellularized pig and mouse lungs were used for exosome isolation. Firstly, the pig was anesthesized using 200mg of Telazol in 2ml of Xylosine by intramuscular injection just above the thigh. Once it was asleep, the ear was searched for veins where the syringe could be inserted. 1ml heparin was injected and after a ten minute wait for the blood to thin, 4ml beuthanasia was injected to put it down. A stethoscope was used to check for any heartbeat. Once this was confirmed, the carcass was taken to the necropsy room. The lungs were harvested by making incisions across the abdomen under the ribs and on the sides of the chest. A lobe of lung tissue was taken from the lung for exosome isolation. The rest was put in the bioreactor for decellularization, using the established protocol. (Mortari et al. 2010)

The lobe harvested from the pig lung was dissected so that sections of distal lung, small airway and large airway were obtained until all lung tissue had been utilized. All samples were homogenized in 1ml of Trizol using the Teflon homogenizer. The same procedure was carried out for the decellularized pig lung.

Lungs were harvested from mice. The lungs were divided so that each tube had half a lung in 1ml Trizol. Decellularized lungs were obtained and also divided in the same way. Tissue was homogenized using the Teflon homogenizer.

Exosome Isolation

The samples were first enriched for exosomes using the Invitrogen Exosome Isolation kit. Briefly, 10ml of each sample was spun at 3000xg for 30 minutes. The supernatant was

transferred to a fresh 15ml conical tube and 0.2 parts, in this case 2ml, of exosome isolation reagent added. After that, the sample was incubated in the cold room (2-8ºC) for 30 minutes. Then the sample was divided into 10 eppendorf tubes with 1ml of sample in each and centrifuged at 10,000xg for 5 minutes. After the supernatant was aspirated, the pellet was resuspended in 100µl of exosome resuspension buffer in each tube. The solution was pipetted up and down and the pellet left to dissolve for 10 minutes at room temperature. The solutions were then combined back into a 15ml conical tube and kept on ice until the RNA isolation step.

Total RNA Isolation from Exosomes

RNA was isolated from the samples using the Invitrogen exosome RNA isolation kit (Life Technologies™, Carlsbad, California). To begin with, the 2X denaturing solution was pre-warmed at 37ºC in a water bath with occasional swirling for 5-10 minutes. The resuspended samples were incubated at room temperature for 5-10 minutes prior to RNA isolation. Then one volume of 2X denaturing solution was added and the sample incubated on ice for 5 minutes. One volume of acid-phenol:chloroform was added. Samples were mixed by vortexing for 30-60 seconds and then centrifuged at 10,000xg for 5 minutes. Two clear layers were formed, with a compact interphase. The upper layer was carefully removed, without touching the interphase. All the aqueous phases were collected in one tube for each sample type. The elution solution provided in the kit was preheated to 95ºC for RNA purification. 1.25 volumes of 100% ethanol was added to the aqueous phase and mixed thoroughly. If the samples were more than 700µl they were

split into separate tubes as this is the maximum capacity of the filter cartridges, which are utilized in the next steps. 700µl of the lysate/ethanol mixture was pipetted onto the filter cartridge and centrifuged at 10,000xg for 15 seconds. This step was repeated until the whole sample was processed. The flow-through was discarded with each step. The sample was washed with 700µl of miRNA Wash Solution 1 and then miRNA Wash Solution 2/3. The samples were centrifuged at 10,000xg for 1 minute to dry the filter and the filter cartridge placed into a new collection tube. 50µl of the pre-heated elution solution was added to the filter cartridge and centrifuged at 10,000xg for 30 seconds. The elution was done twice to end up with 100µl of purified RNA.

RNA quantification

RNA content was measured using a spectrophotometer (Implen nanophotometer® P330). The cuvette was placed inside the device using Lid10 and 1µl elution solution as a blank. Then 1µl of each sample was placed onto the glass spot in the middle of the cuvette and the lid placed on top. The RNA content was measured. The lid and cuvette were cleaned with 75% ethanol between each measurement. An A260/A280 reading of 2.0 would indicate high RNA purity, as stated previously. The RNA samples were stored at -80ºC for further analyses.

RNA Analysis

The isolated RNA samples were then characterized using automated RNA electrophoresis (Experion™ Automated Electrophoresis System) and the Experion RNA StdSens Analysis kit by Bio-Rad. The RNA samples and ladder aliquot were thawed on ice and the reagents allowed to equilibriate to room temperature. The kit comes with two

cleaning chips; one for electrode cleaner (EC) and the other for DEPC-treated water washes. The machine was washed with both EC and DEPC-treated water. Afterwards, the gel solution was prepared and combined with 1µl of stain solution. 9µl of the gel-stain solution was loaded onto the chip which was then placed in the priming station. After priming was complete, the chip was checked for any trapped air bubbles or incomplete priming. About 3µl of ladder and samples were transferred into fresh microcentrifuge tubes which were incubated at 70ºC for 2 minutes to denature the RNA strands and then kept on ice for 5 minutes. They were spun down and kept on ice until the chip was loaded. The chip was then loaded with another 9µl of gel-stain solution in the upper GS well followed by 9µl of filtered gel solution in the G well. 5µl of loading buffer was pipetted into all the sample wells including the ladder well. 1µl of ladder was pippeted into the L well and 1µl of sample into each respective sample well. The chip was placed in the Experion vortex station for 1 minute. It was important to make sure the chip was run 5 minutes within loading the samples. The chip was placed in the electrophoresis station and the Eukaryotic RNA StdSens Assay chosen which detects total eukaryotic RNA. The chip was discarded when the run was complete and the electrodes rinsed with DEPC-treated water. The images of all spectra, the virtual gel and the RNA quality index (RQI) of all samples were recorded.

The whole RNA analysis was repeated for the decellularized pig and mouse lung samples but this time the decellularized samples were done in duplicate to get a total of eight samples.

Finally, a total RNA sample from normal pig lung was run on the chip to observe the typical peaks seen for cellular samples. The RNA was isolated using the Invitrogen protocol with Trizol reagent.

Reverse Transcription of miRNA

Reverse transcription was performed using six primers of miRNAs that are known to have a role in lung development using the Applied Biosystems miRNA reverse transcription kit.

Two of them, miR 17 and snoRNA202 were chosen as positive endogenous controls for the qRT-PCR since they are known to be stably expressed in both mouse and pig tissue. The other primers tested were miR15a, miR375, miR29b and miR29c (Applied Biosystems®, Grand Island, NY).

Briefly, a master mix was prepared for 26 reactions which would be equivalent to two primers plus a reaction to compensate for possible pipetting errors The thermocycler has a limited capacity for PCR tubes so the samples were reverse transcribed in pairs. The amount of each reagent stated in the protocol was multiplied for 27 reactions, allowing extra volume for pipetting errors. Briefly, 112.32µl of nuclease-free water was pipetted into a 600µl microcentrifuge tube along with 40.5µl of 10X RT(reverse transcription) buffer, 27µl of Multiscribe™ RT enzyme, 5.13µl of RNase inhibitor and 4.05µl of dNTP mix. The resulting master mix was centrifuged for ten seconds to bring all the solution to the bottom of the tube. The first two reverse transcription reactions were run using primers sno202 and miR17 which would ultimately be used as the endogenous controls in the qRT-PCR reaction. 7µl of master mix was pipetted into each PCR tube followed by

5µl of RNA sample into the respective tubes. Afterwards, 3µl of the 5X RT primers were added to the mixture and all tubes were centrifuged for about ten seconds to bring all the solution to the bottom. The thermal cycler was run with the following conditions: HOLD at 16ºC for 30 minutes, HOLD at 42ºC for 30 minutes and finally HOLD at 85ºC for 5 minutes. The machine then holds the samples at 4ºC until collection. This was done for miR15a and miR29b in the second round of reverse transcription and miR29c and miR375 in the third round. The samples were stored at -20ºC until further analysis.

Probe	Known Functions
sno202	Housekeeping gene
miR17	Housekeeping gene
miR15a	Cell cycle regulation
miR29b	Regulation of ECM deposition and remodeling
miR29c	Unknown
miR375	Differentiation to definitive endoderm/development of endoderm

Table 1: Probes used for real-time PCR analysis of exosome miRNA and their known functions.

Measurement of copyDNA(cDNA) content

The cDNA content of the samples were measured using the spectrophotometer (Implen nanophotometer® P330). The program was set to nucleic acids then single-stranded DNA and the concentration, A260/280 and A260/230 values were recorded. An A260/280 ratio of at least 1.8 and an A260/230 ratio between 2.0 and 2.2 are indicators of good quality DNA. Phenolic contaminants such as Trizol will absorb at both 230nm and 280nm and proteins absorb highly at 280nm. Other contaminants such as EDTA and carbohydrates absorb highly at 230nm so if the sample has a high absorbance at 260nm compared to

280nm and 230nm then a good ratio will appear. Nuclease-free water was used as a blank. 1µl of each sample were used to measure DNA concentration.

Real-time RT-PCR

Firstly, the cDNA from the reverse transcription was tested to see if it required any dilution. The qRT-PCR instrument is very sensitive and can detect amounts of cDNA as low as the picogram level. Therefore, 1-100ng cDNA is the ideal range that should be aimed for. According to the cDNA concentrations generated from reverse transcription, the ideal amount of total cDNA would be obtained if 1.33µl of RT product is put in a 20µl PCR reaction. Therefore, the experiment was conducted without any cDNA dilution. Prior to commencing the experiment, a template was prepared for the 96-well plate on Applied Biosystems software for the PCR run.

10µl of Taqman Universal Master Mix and 7.67µl of nuclease-free water is required for each well. Four wells were used as 'no template controls' and contained 10µl of master mix and 10µl of nuclease-free water. 1µl of each Taqman probe and 1.33µl of each cDNA sample were added to the designated sample wells. After centrifuging the plate at 1,000xg for one minute, to ensure all of the samples were brought from the sides of the wells to the bottom, it was then placed in the PCR instrument and run using the following conditions: 50ºC for 2 minutes, 95ºC for 10 minutes, 95ºC for 15 seconds (40 cycles) and 60ºC for 1 minute. The data was analyzed using ABI software and all mouse samples were normalized to non-decellularized mouse lung and all pig samples normalized to non-decellularized distal pig lung.

Bradford Assay

Exosomes also contain a significant amount of protein. The Bradford assay exploits a blue dye in the Bradford reagent, called brilliant blue G which binds to proteins and changes the absorption maximum of the dye. Bovine serum albumin (BSA) is used as a standard reference protein in these assays. A serial dilution of the BSA was made to plot a standard curve. 1:5 dilutions of the exosome samples were used and the absorbance was measured at 595nm.

iPSC culture to definitive endoderm

Isolation of exosomes for cell culture

Exosomes were isolated from decellularized pig lung by dissection of distal parts of the lung followed by homogenization of the tissue as previously described. Exosomes were isolated using an exosome isolation kit for serum (Invitrogen™, Carlsbad, California). The resulting sample was filtered using a 0.22μm from Millipore to avoid contamination of the cell culture. The approximate amount of exosomes was measured by quantifying the amount of protein in the sample using the Bradford assay.

Cell Culture

Passage 14 human iPSCs (courtesy of Dr. Nobuaki Kikyo's laboratory, Stem Cell Institute, University of Minnesota, Minneapolis, MN) that were grown on Geltrex (Invitrogen™, Carlsbad, California) were used for differentiation to definitive endoderm. A 12-well plate was prepared with the first group designated to the differentiation of iPSCs to definitive endoderm with exosomes added. The second group was for iPSC

differentiation to definitive endoderm without exosomes and the last group was used as a negative control, namely iPSCs cultured in essential 8 medium for their maintenance (Table 2). Samples were taken at day 0 and day 6 from each quadruplicate for RNA analysis and gene expression.

	Differentiation Factor	Exosomes	Anticipated Result
1	Basal differentiation media, Act, Wnt, β-mercaptoethanol, FBS	+	Change in cell phenotype different from group 2
2	Act, Wnt, β-mercaptoethanol, FBS	-	Change in cell phenotype
3	None	-	No change, remain as undifferentiated iPSCs

Table 2: Experiment setup for iPSC culture to definitive endoderm

At day 2.5, pictures of each well were taken using bright field microscopy (Leica Microsystems, DMI 3000) before the media change. All wells were subjected to a half media change. The same procedure was carried out on day 5.

On the last day of cell culture (day 6), pictures of each well were taken using brightfield microscopy (Leica Microsystems, DMI 3000). Then 1ml of Trizol reagent was put into the wells and pipetted up and down to make sure the cells mixed with the Trizol reagent. Finally, this mixture was pooled for each row of wells into 15ml conical tubes for RNA and gene expression analysis.

RNA isolation and purification

RNA was isolated in the same way as it was done in the bioreactor experiment using Trizol reagent (Invitrogen™, Carlsbad, California). RNA purification was also done as previously using the RNA mini kit (Invitrogen™, Carlsbad, California).

Automated gel electrophoresis

This was done the same way as for the normal and decellularized lung miRNA samples. Cell culture samples were done in triplicate in the 12-well chip.

Reverse Transcription

RNA was converted to cDNA using the SuperScript® III first-strand synthesis for qRT-PCR (Invitrogen™, Carlsbad, California), same as the bioreactor samples.

qRT-PCR of cell culture samples

This part was carried out in the same way as qRT-PCR was done for the samples from the bioreactor experiment. The probes used included markers for undifferentiated iPSCs, definitive endoderm and more mature lung cell markers as shown in Table 3 below.

Probe Name	Known Function
Oct 2	Maintains pluripotency in iPSCs
Sox 4	Maintains pluripotency in iPSCs
Nanog	Maintains pluripotency in iPSCs
Vimentin	Intermediate-filament protein. Marker of mesenchymally-derived cells
Pax8	Required for endoderm formation
Pdx1	Definitive endoderm marker
FoxA2	Definitive endoderm marker
Sox17	Definitive endoderm marker
SPC	Surfactant protein C, found in type II pneumocytes
AQP5	Aquaporin 5 is found in type I pneumocytes
CC10	Club cell marker found in small airway epithelia
FoxJ1	Required for cilia formation in airway and alveolar epithelial cells
TTF1	Role in lung morphogenesis and regulation of surfactant proteins, found in type II pneumocytes and non-ciliated bronchiolar epithelial cells
Sox9	Lung morphogenesis, distal progenitor marker
p63	Transcription factor involved in lung development
CK5	Keratin protein expressed in epithelial tissue

Table 3: Markers used in real-time PCR of samples from iPSC culture to definitive endoderm

RESULTS

Cell Count

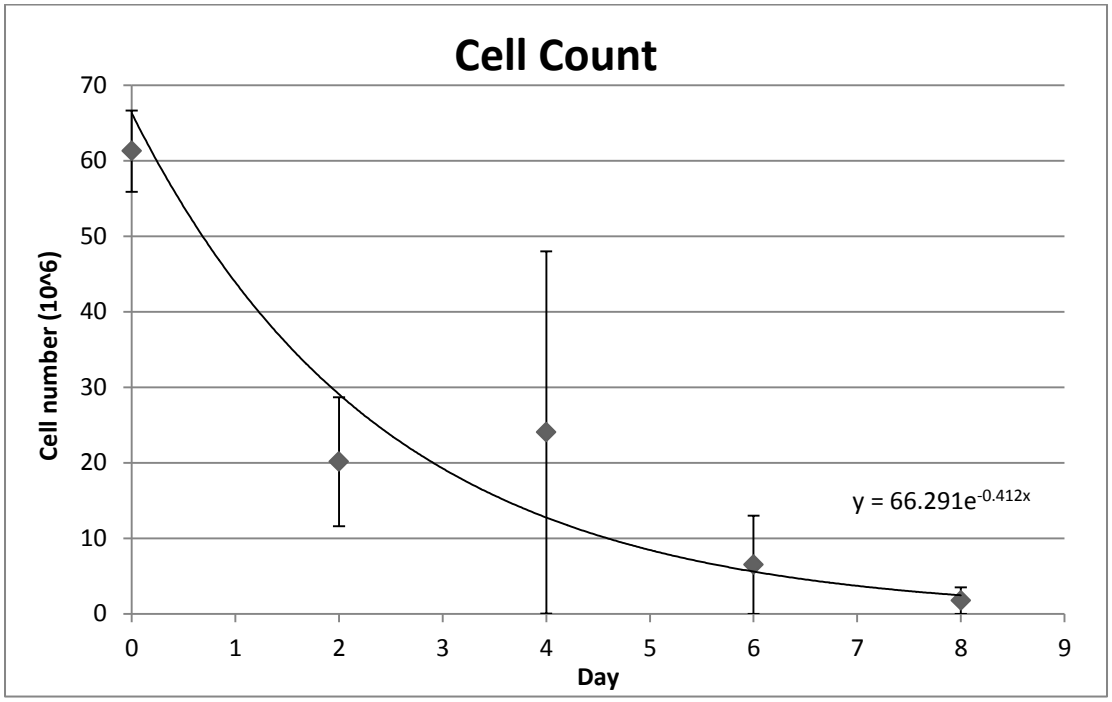

Figure 2: Number of cells and how they changed over 8 days of culture in stirred flask bioreactor. Error was calculated using standard error (Cumming et al, 2007)

The cell count at day 0 was 52.3 million cells. This value rapidly decreased to 20 million upon commencement of culture in stirred flask bioreactor. This is expected in the transition from 2D to 3D culture as the latter has low oxygen levels that the cells have to adjust to. Consequently, cell numbers increased back to 72 million on day 4, indicating adaptation to 3D culture conditions. Usually, cell numbers would continue to increase until cell passage is required. On the contrary, cell numbers drop rapidly to 20 million on day 6 and 5.25 million on day 8. This is an indicator of unsuitable 3D culture conditions. The iPSCs need extra support in the form of a matrix or additional growth factors.

RNA isolation and agarose gel electrophoresis

No detectable RNA was found by the RNA isolation method in any of the samples from the stirred flask bioreactor culture but agarose gel electrophoresis was still carried out to check if GAPDH was present and if any RNA was isolated. No RNA appeared in the lane for GAPDH but only the ladder was clearly visible (Figure 3), indicating that the gel was run correctly but there must have been a flaw in the amplification of GAPDH or that the cells were dead. Alternatively, the RNA isolation was not done properly and was lost in processing.

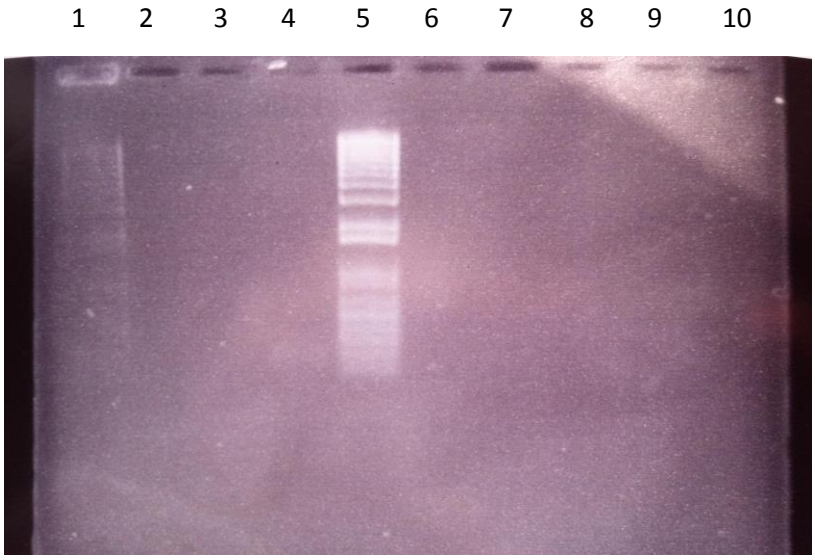

Figure 3: Image of agarose gel faintly showing the ladder in lanes 1 and 5

Lactate Assay

The lactate assay gave a linear standard curve, as expected. There are a couple of outliers but they were not far from the standard curve line. As the lactate concentration increased,

the absorbance of the standards at OD570 increased by the same amount which can also be seen in Table 4. This demonstrates the linearity of relationship between lactate concentration and absorbance at 570nm as shown below in Figure 4 (upper figure).

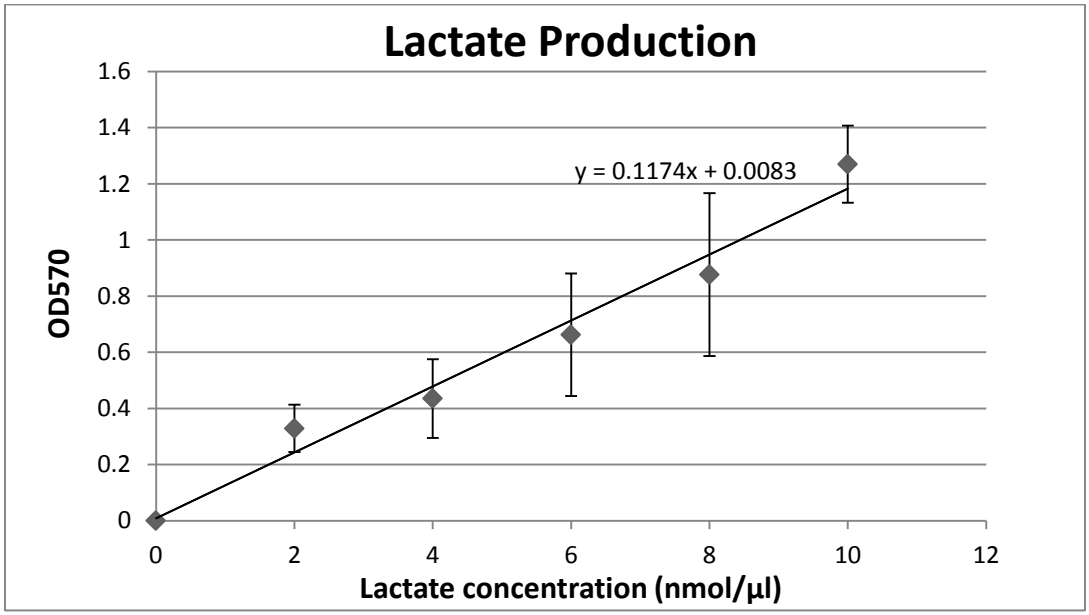

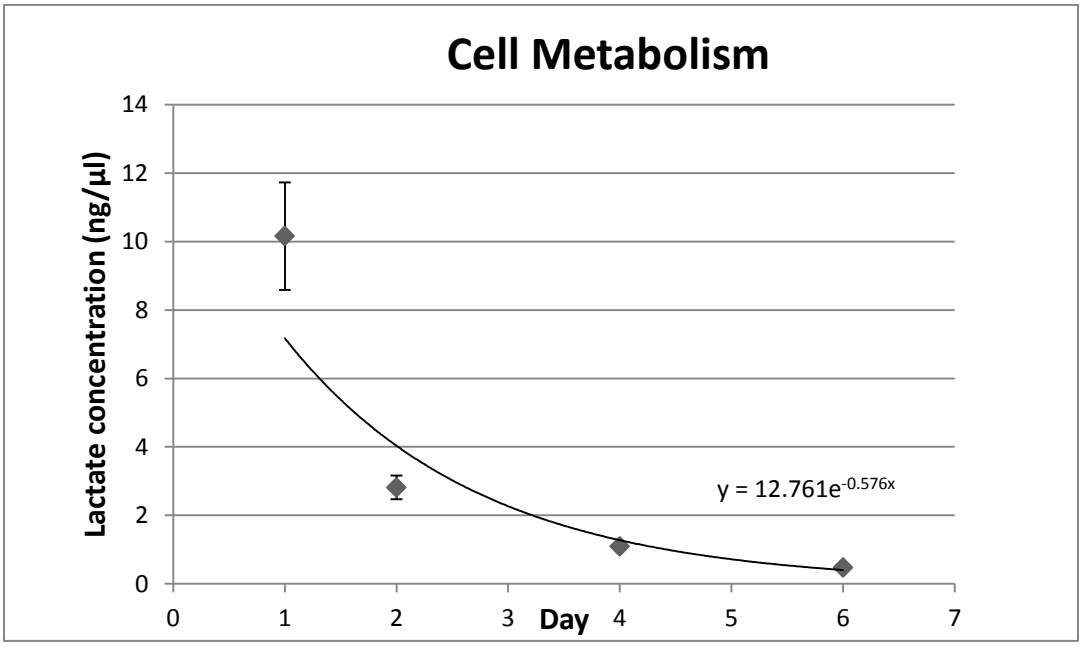

Figure 4A: Set of standard concentrations for lactate assay. 4B: Lactate levels in 3D cell culture over the course of 6 days. Error bars for both graphs are calculated using standard error with n=3 (Cumming et al, 2007)

An equation was generated from the standard curve and used to determine the lactate concentration in the samples tested, which were from days 1, 2, 4 and 6 of the stirred suspension culture. Table 4 shows the calculated lactate concentrations for all the different absorbance values generated at 570nm for different sample solution strengths. The first column shows a 25-fold dilution and the second column a 12.5 dilution and so on. The 6.25-fold dilution was picked for analysis as these values all fell in the linear part of the curve. A graph of lactate concentration versus day was plotted to better visualize the changes in lactate concentration from days 1-6 (Figure 4, lower figure). According to the graph, lactate concentrations were very high on the first day followed by a big drop on the second day and then a slower, more gradual decrease after day 2 until day 6. This indicates that the cells were producing lactate on the first day and the dramatic decrease points to the sudden cell death observed. Any remaining cells then slowly diminished after day 2.

	Volume in 50 µl	2	4	6	8	10
	d1	2.99	4.85	7.07	11.2	12.2
	d2	0.9	1.66	2.27	2.71	3.47
	d4	0.43	0.77	1	1.03	1.25
Lactate concentration (ng/µl)	d6	0.26	0.39	0.49	0.49	0.44

Table 4: Calculated lactate concentrations of bioreactor samples at days 1, 2, 4 and 6 with various dilutions shown in row 1.

Glucose Assay

The curve generated from the standard set of concentrations was completely linear (Figure 5). The absorbance values at 540nm were directly proportional to the glucose concentration in the standard solution.

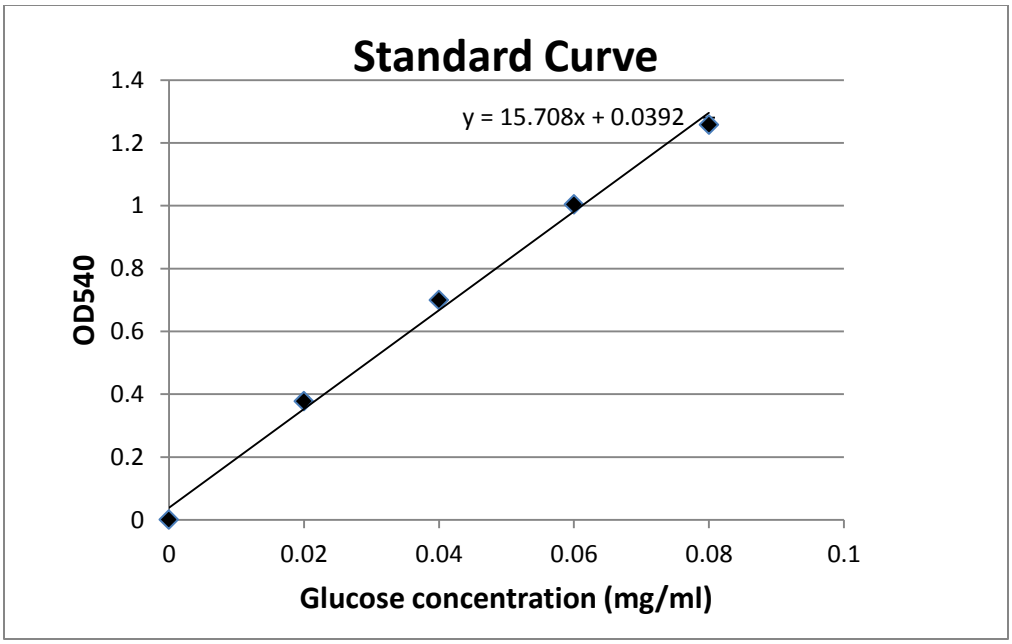

Figure 5: Set of standards for glucose assay. Error bars using standard error with n=3 (Cumming et al, 2007)

As in the lactate assay, the equation of the standard curve was used to determine the glucose concentrations of bioreactor samples. The absorbance values were substituted as the y-values in the equation to find the x-values. The results were then multiplied by 100 as the dilution was 1:100 (Table 5).

Day	Absorbance value at 540nm	Glucose Concentration (mg/ml)
0	0.096	0.29
2	0.587	3.52
4	0.261	1.38

Table 5: Determined glucose concentrations for bioreactor

RNA isolation from exosomes

Exosomes were isolated successfully from normal and decellularized pig and mouse lung tissue followed by RNA isolation. The exosome isolation was determined successful by checking for the presence of a small gel-like pellet during the last 10,000xg centrifugation step of the exosome isolation protocol. In some cases, it was not be visible however some of the samples showed evidence of this pellet. Nevertheless, this is not enough to confidently say there are exosomes in the samples. Further analysis is required by identifying the RNA and protein content of these vesicles.

RNA concentration measurement

The RNA concentrations were measured using the Implen nanophotometer® P330 (Table 4). The large airway of the normal pig lungs have the highest RNA concentration followed by pig distal lung, mouse lung and finally the pig small airway controls. In both of the decellularized lung samples 1 and 2, pig distal lung had the highest RNA concentration followed by small airway, mouse lung and finally, large airway. It is not a surprise that the normal lung samples had much higher RNA concentrations than their decellularized counterparts. It may be possible that the large airway sample obtained happened to have the largest amount of RNA due to the amount of tissue extracted. Since the normal lung samples were only processed once, it would not be possible to confirm this until the experiment is repeated for these normal lung samples.

There were differences in RNA content between the first and second sets of lungs with the first having higher concentrations of RNA for mouse, pig alveolar and large airway. The pig distal lung among the first batch of decellularized lungs had an unusually high concentration of RNA which could be partially explained by the low RNA purity. If an RNA sample is not pure or clean, the concentration value will be abnormally high due to the absorption of impurities such as proteins. Proteins absorb at the same wavelength as RNA so the concentration value can be misleading however the A260/280 ratio is helpful in these cases. The results for the second set of lungs were reproducible in that they had similar RNA concentrations to the first batch. The A260/A280 ratios represent RNA purity in that A260 means absorbance at 260nm and A280 means absorbance at 280nm wavelengths. Nucleic acids typically absorb at 260nm and contaminants such as Trizol used in the RNA isolation processes absorb at 280nm. Therefore, an absorption spectrum would have a peak at 260nm that is twice as high as the peak at 280nm, giving a ratio of 2. The ratios that are 2.0 or higher would qualify as ultra pure RNA and ratios of 1.8 would be acceptable quality. However, ratios below 1.8 would be classified as poor quality RNA. Referring to Table 4, all the normal lung samples have ultra pure RNA. The first batch of decellularized lung samples did not yield high quality RNA but the second batch had ultra-pure RNA for mouse lung, small airway, large airway and distal pig lung had acceptable RNA purity. The overall RNA quality was much better for the second batch of decellularized lungs.

Automated RNA electrophoresis

After determining the purity of the RNA, the next step was to investigate what kind of RNA was isolated. As exosomes are highly enriched for miRNA, the presence of high amounts of these short sequence nucleotides would indicate that, indeed what was isolated were exosomes. The same sets of lungs were used as for the RNA concentration measurements. Figure 6 shows the results for the ladder appeared as expected, with its 9 characteristic peaks of certain shape and height. The RNA peaks in this experimental method are specific to the type of RNA present. MicroRNA typically appears at the early part of the experiment (between 25 and 35 seconds) so the peaks on the left-hand side of the graph were broader compared to the earlier peaks. The height of the peak represents the amount of miRNA present.

Sample	RNA concentration (µg/ml)	A260/A280
Normal mouse lung	433	2.146
Decellularized mouse lung (1st batch)	8.748	1.600
Decellularized mouse lung (2nd batch)	8.35	2.300
Normal distal pig lung	413	2.149
Decellularized distal pig lung (1st batch)	117	1.500
Decellularized distal pig lung (2nd batch)	11.5	1.812
Normal small airway	102	2.246
Decellularized small airway (1st batch)	22.7	1.500
Decellularized small airway (2nd batch)	9.940	2.273
Normal large airway	473	2.138
Decellularized large airway (1st batch)	7.157	1.200
Decellularized large airway (2nd batch)	7.157	2.000

Table 6: RNA concentrations and purity measures for normal and decellularized mouse and pig lungs.

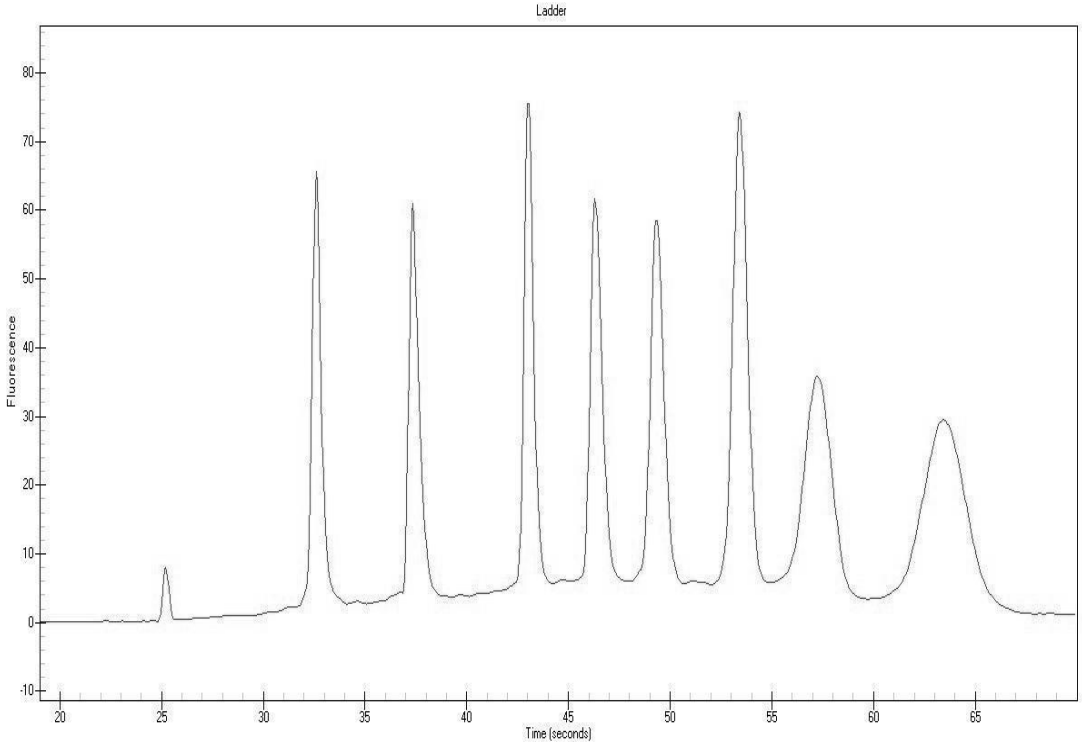

Figure 6: RNA ladder for automated gel electrophoresis

The automated RNA electrophoresis method uses a fluorescent dye to measure the amount of RNA in a particular sample. The samples are pipetted into a tiny chip with microfluidic channels at the bottom. When the electrodes in the device come in contact with the fluid in the chip, a current is generated, which initiates the process of small molecule migration similar to agarose gel electrophoresis or SDS-PAGE. The smaller the molecule, the faster it will migrate. Therefore, the first RNA molecules to appear on the graph will be the small RNAs such as microRNAs and long non-coding RNAs. This will be followed by messenger RNA and then the respective ribosomal RNAs, depending on the species being tested. The heights of the peaks will vary depending on the fluorescence intensity, which directly represents the amount of that particular type of RNA. The first

small peak in the graph represents a reference peak which the device uses as a base value when generating the other peaks.

The peaks have a definite shape, height and size and the ladder provided in the kit is a set of RNA molecules of known molecular weight. They are known to produce defined peaks as above. The first six peaks are narrow and sharp while the last two are smaller and broader. According to the data provided by BioRad™, the peaks in Figure 6 appeared in the expected manner. This ladder can be used to estimate the molecular weights of unknown samples of RNA.

Figure 7: Automated RNA electrophoresis spectra for normal lung samples. Arrows indicate the peaks for miRNAs. The area under these peaks from 25 to 35 seconds is the time for miRNA appearance.

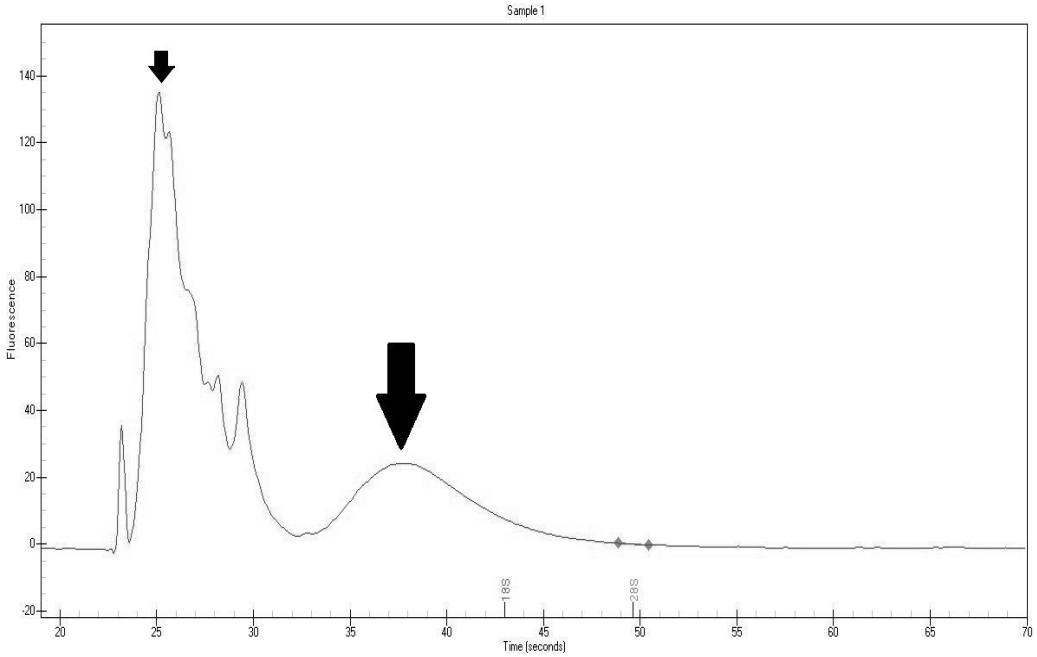

Figure 7A: Automated RNA electrophoresis spectrum for normal mouse lung

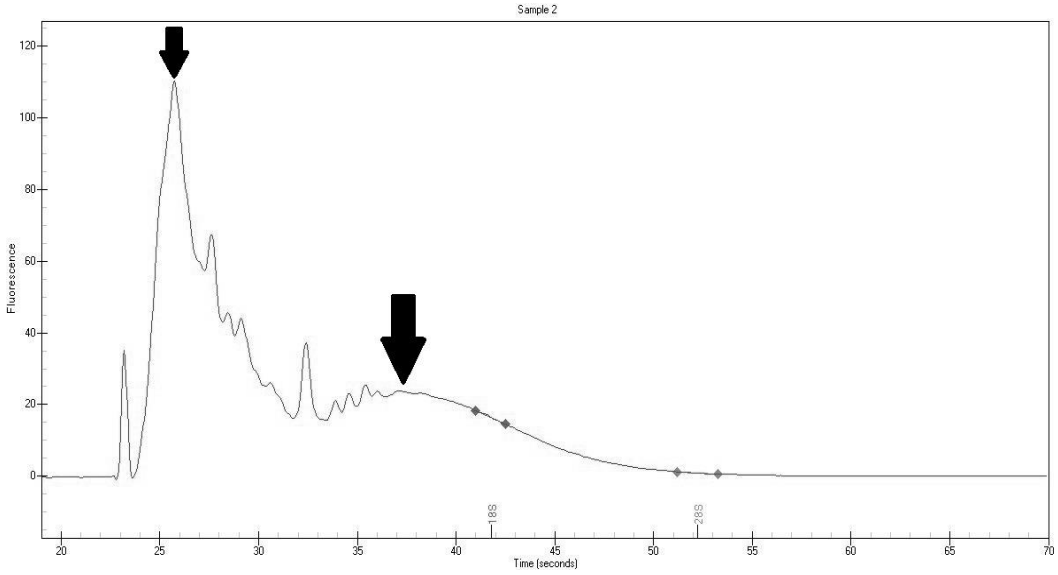

Figure 7B: Automated RNA electrophoresis spectrum for normal pig distal lung

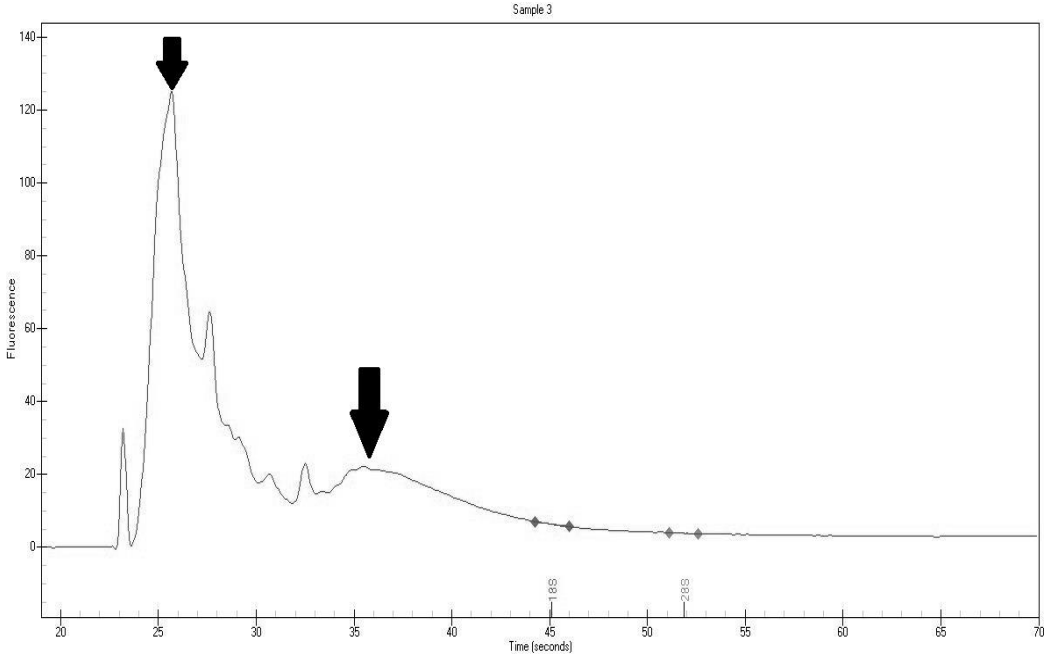

Figure 7C: Automated RNA electrophoresis spectrum for normal pig small airway

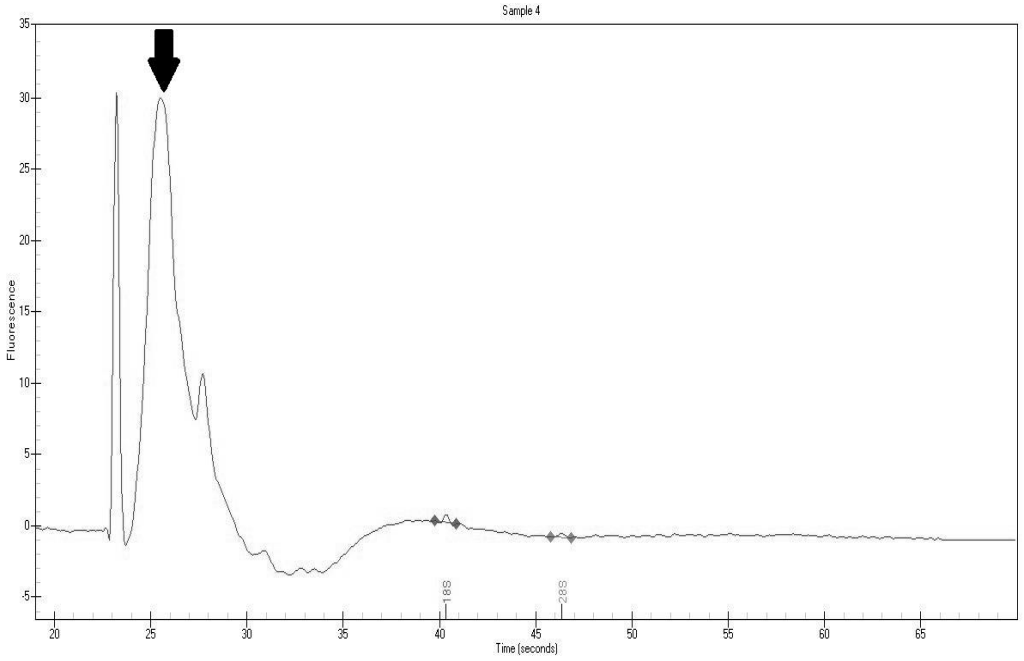

Figure 7D: Automated RNA electrophoresis spectrum for normal pig large airway

According to Figure 7, there is a high amount of small, short sequence RNAs for all normal lung samples. The next smaller but broader hump shows the typical peak for mRNAs, which is a common component of normal lungs (2^{nd} arrow in Figures 7A, B and C). The large amount of exosomes found in all normal lung samples are due to the presence of cells which contain MVBs. These are the main source of exosomes therefore a high level of fluorescence is observed for all normal lung samples. The wider peaks indicate the presence of more RNA sequences of different lengths. The pairs of dots further to the right represent the 18S and 28S ribosomal RNA peaks. Cellular samples would have tall, sharp peaks at both these points like in Figure 7E. Since exosomes were isolated before automated gel electrophoresis, these sharp peaks are absent in Figures 7A-D. This indicates that the sample did not contain 18S or 28S rRNA. In contrast, Figure 7E shows that the 18S and 28S peaks are clear and sharp when cellular RNA is run on the chip.

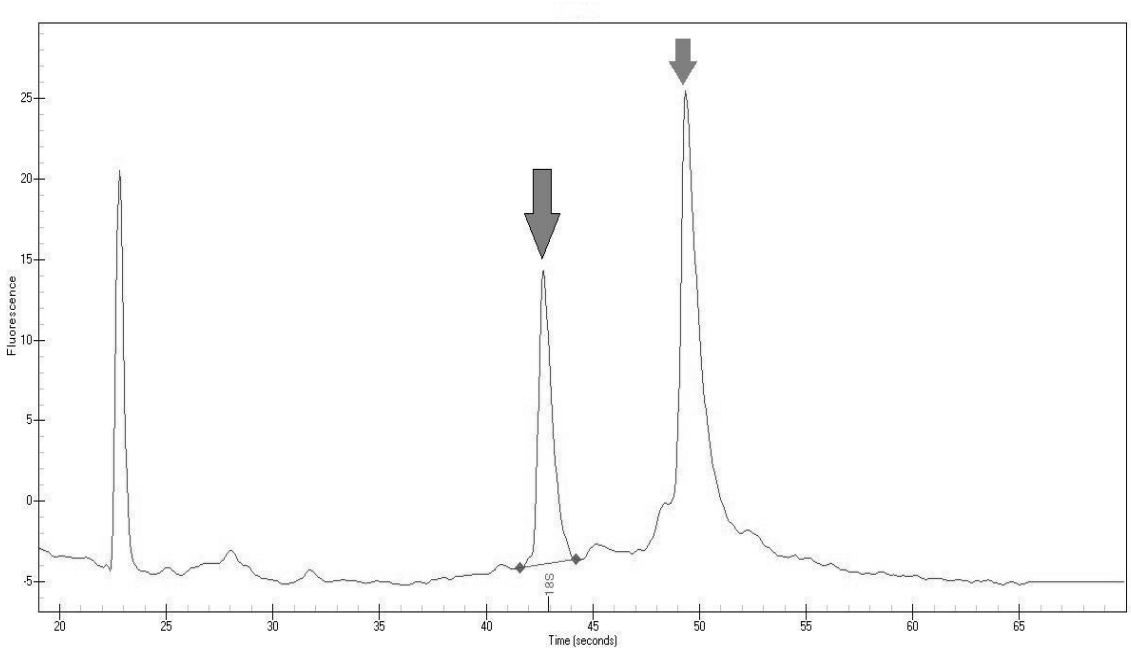

Figure 7E: Automated electrophoresis spectrum for normal pig lung. Arrows indicate the 18S on the left and 28S peak on the right.

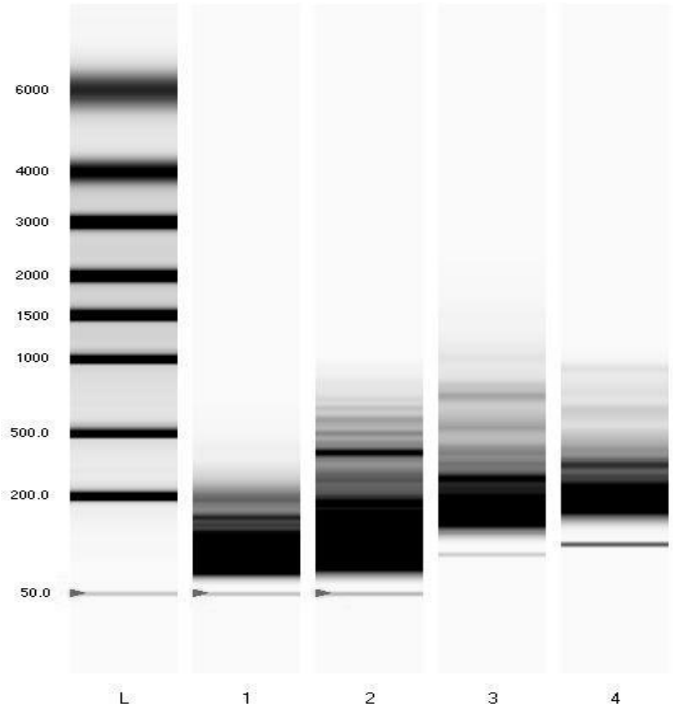

Figure 8: Virtual gel image of RNA from normal lung samples generated by the Experion automated electrophoresis instrument. From left to right: L-Ladder, 1-mouse lung, 2-pig distal, 3-pig small airway, 4-pig large airway

The bands in lanes 1-4 (Figure 8) are very clear-cut and thick which reflects the tall peaks seen in all normal lung samples (Figures 7A-D). This indicates the presence of significant amounts of miRNA in all normal lung samples.

Figure 9: Automated RNA electrophoresis for 1st set of decellularized pig and mouse lungs. A: mouse, B: pig alveolar, C: pig small airway, D: pig large airway

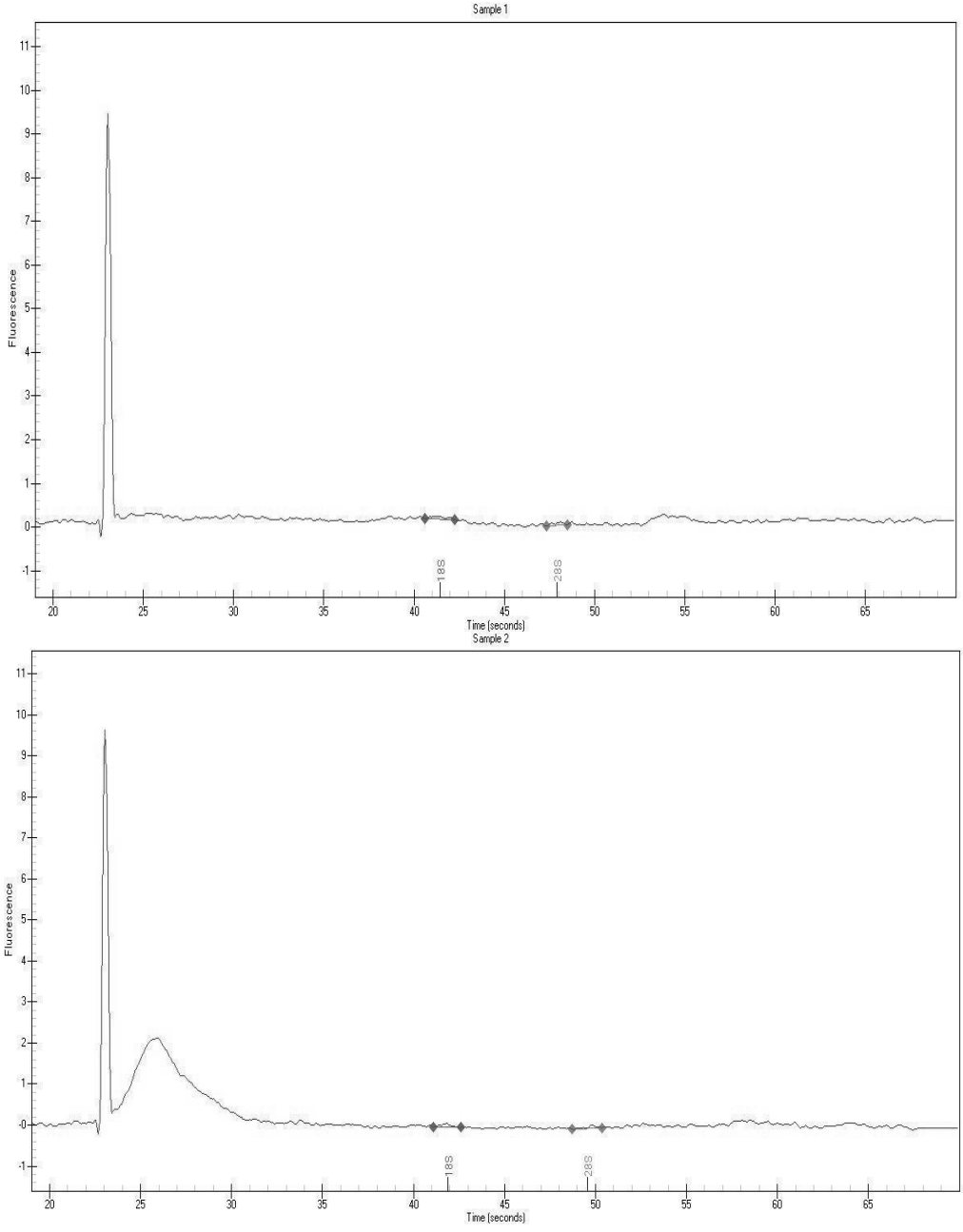

Figures 9A and 9B

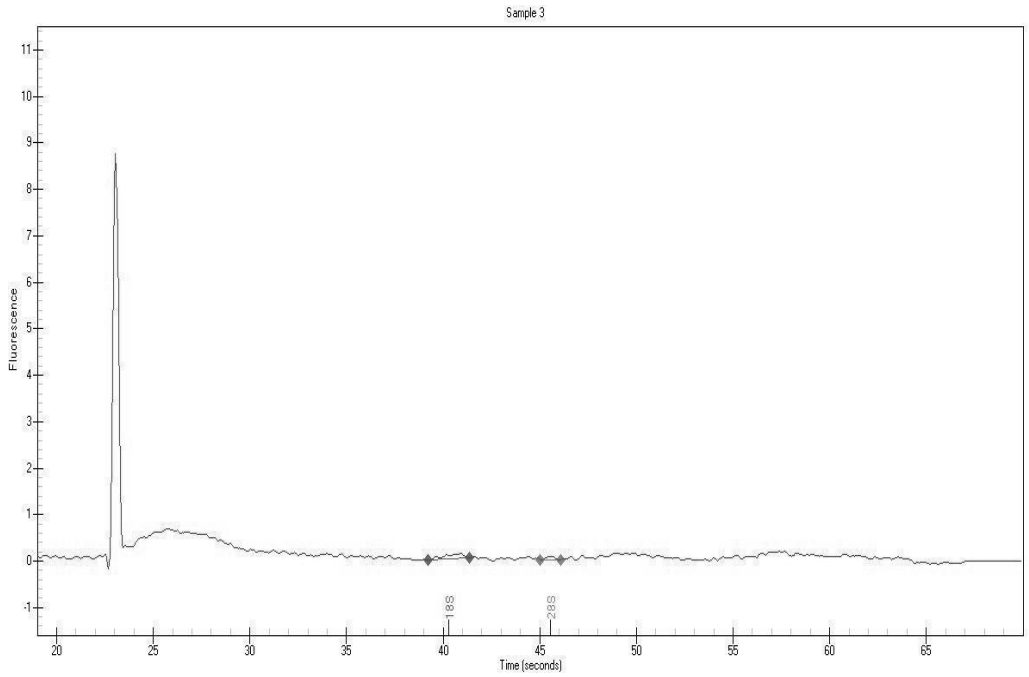

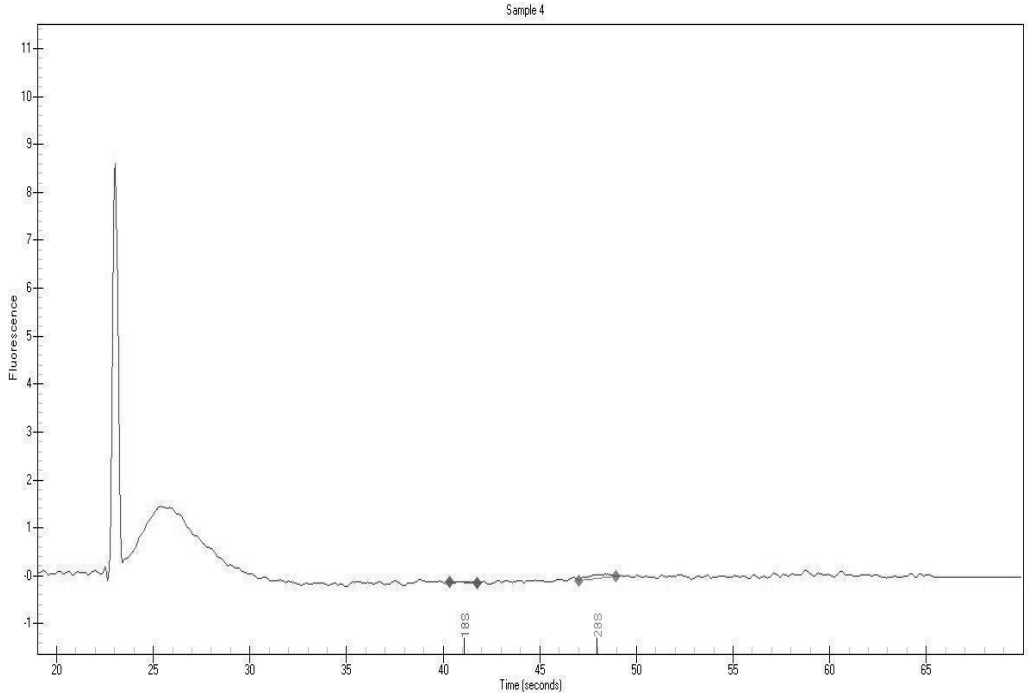

Figures 9C and 9D

The decellularized mouse lung did not give rise to any significant peak (Figure 9A) however the pig lungs did, with the alveolar or distal region having the largest peak (Figure 9B). The large airway and the small airway had smaller peaks (Figures 9C and D). This does not correlate with the RNA concentrations obtained during the RNA isolation step (Table 5). The reference peaks appear in the expected places which are 20-25 seconds and 8-10 fluorescence units. The 18S and 28S ribosomal RNA peaks do not appear which demonstrates successful exosome isolation. There is also no mRNA hump straight after the small RNA region which also strongly indicates that the RNA peaks belong exclusively to exosomes.

Figure 10: Automated RNA electrophoresis results for 2nd set of decellularized pig and mouse lungs. A: mouse, B: pig alveolar, C: pig small airway and D: pig large airway

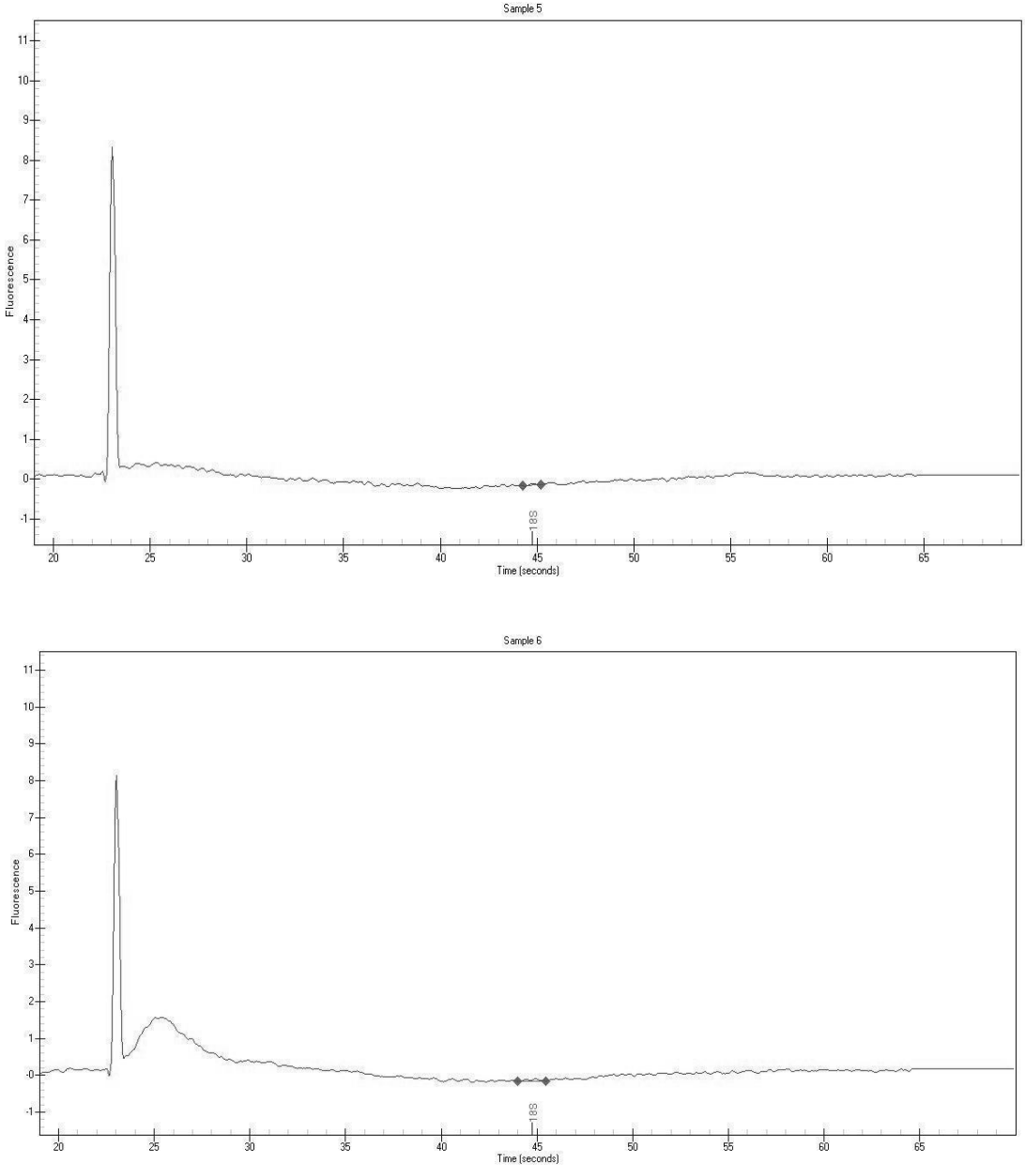

Figure 10A and Figure 10B

The second batch of decellularized mouse lung also showed no significant level of fluorescence (Figure 10A). The pig alveolar sample had the highest fluorescence peak (Figure 10B). This time, however, the large and small airway samples had approximately the same amount of fluorescence (Figures 10C and 10D). The overall heights of the peaks were also much lower than the first set of decellularized lungs. This may explain the unusually high RNA concentrations for the first set of decellularized lungs, giving rise to large peaks in the electrophoresis charts. Their A260/A280 ratios were low which indicates contamination so the RNA peaks in Figure 9 were higher than the actual amount of RNA. This may be the reason for the lower peaks in Figure 10, as the RNA content was very pure and produced a more realistic amount of the RNA quantity. The reference peaks appeared at the right time, between 20 and 25 seconds on the chart and at the right fluorescence level between 7 and 8 units.

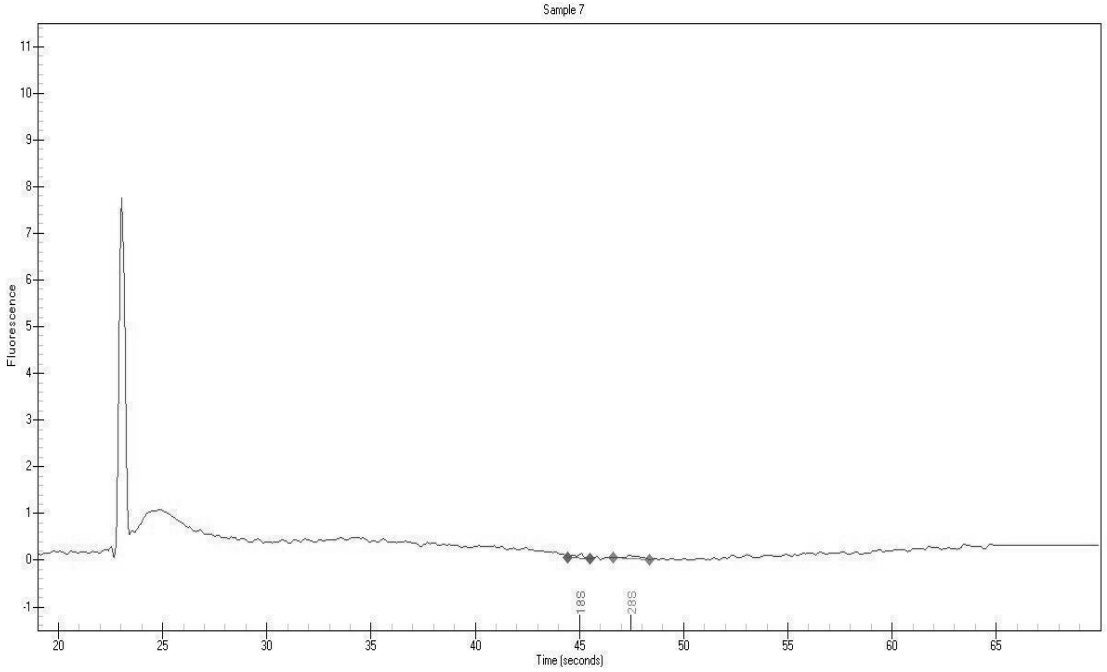

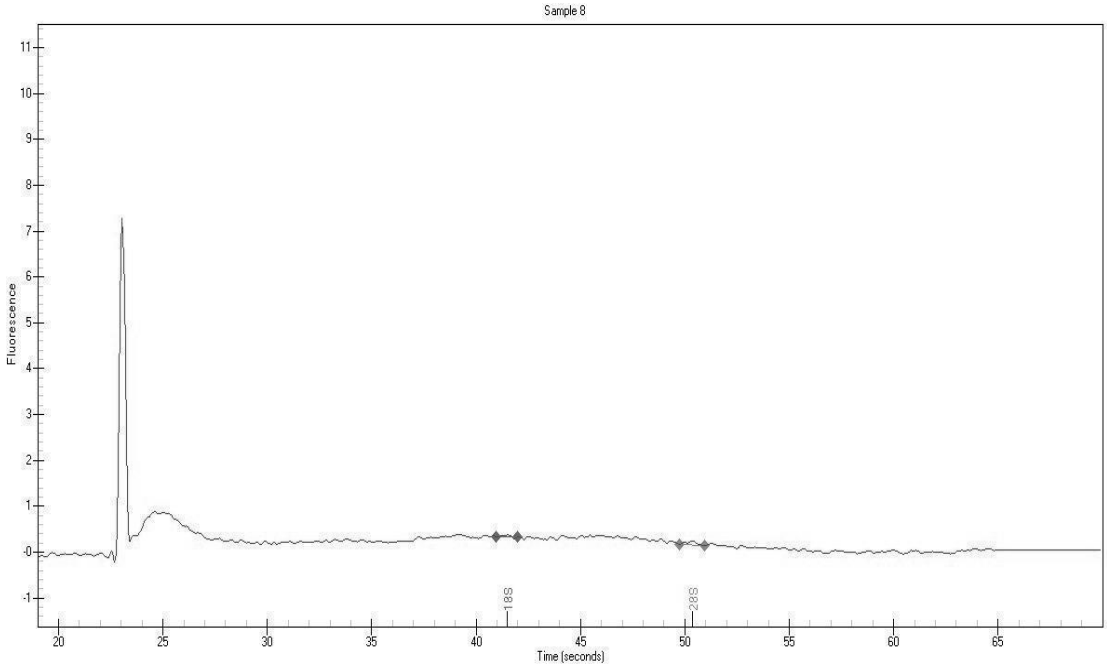

Figures 10C and 10D

Figure 11: Automated RNA electrophoresis results for DEPC-treated water

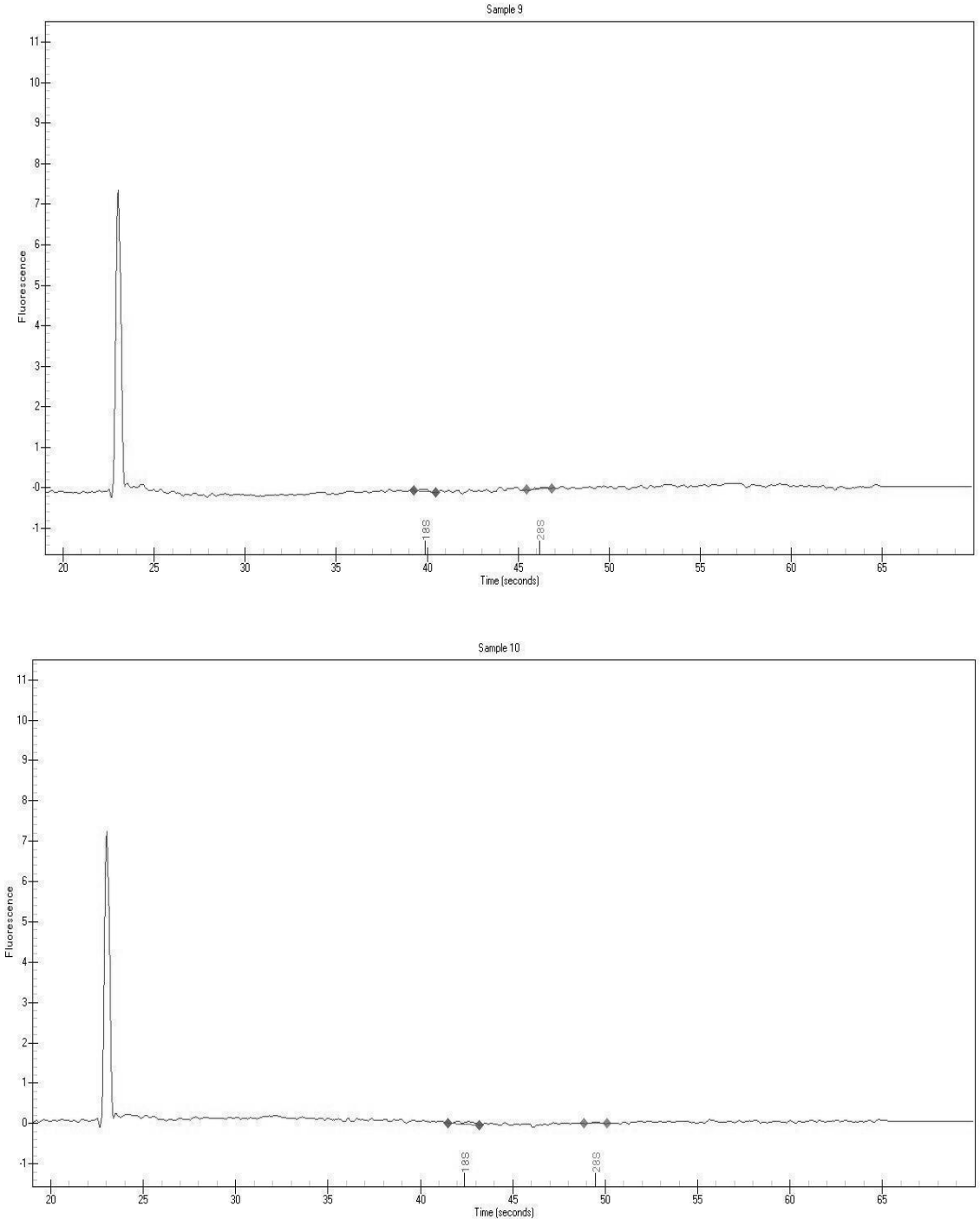

Figures 11A and 11B

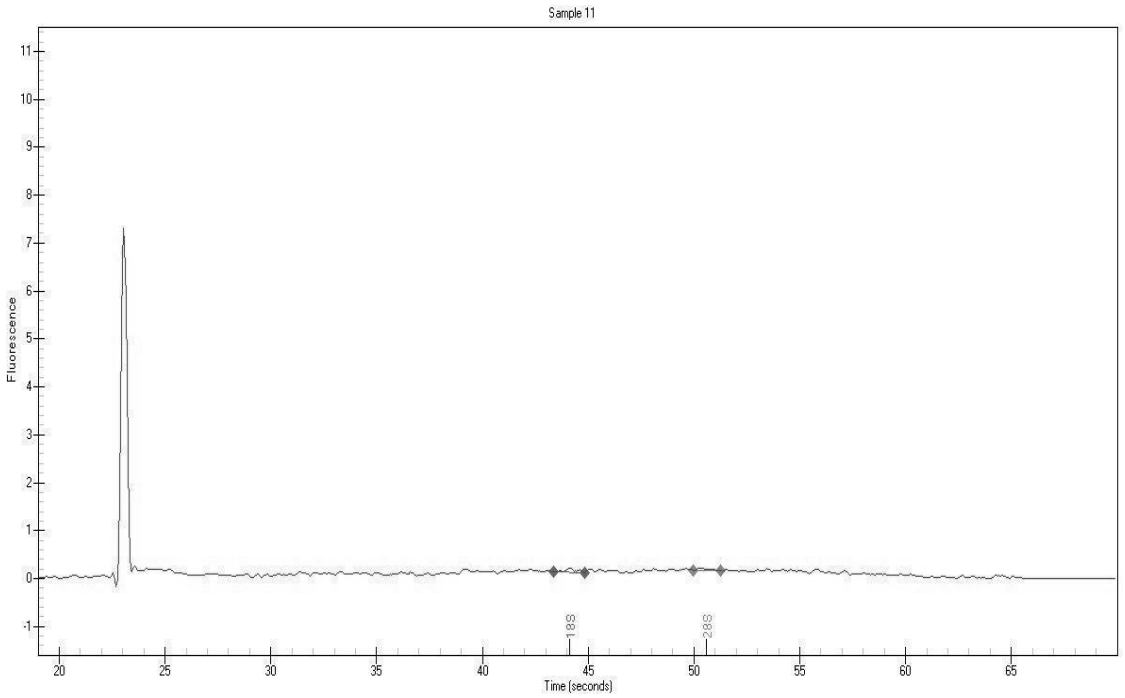

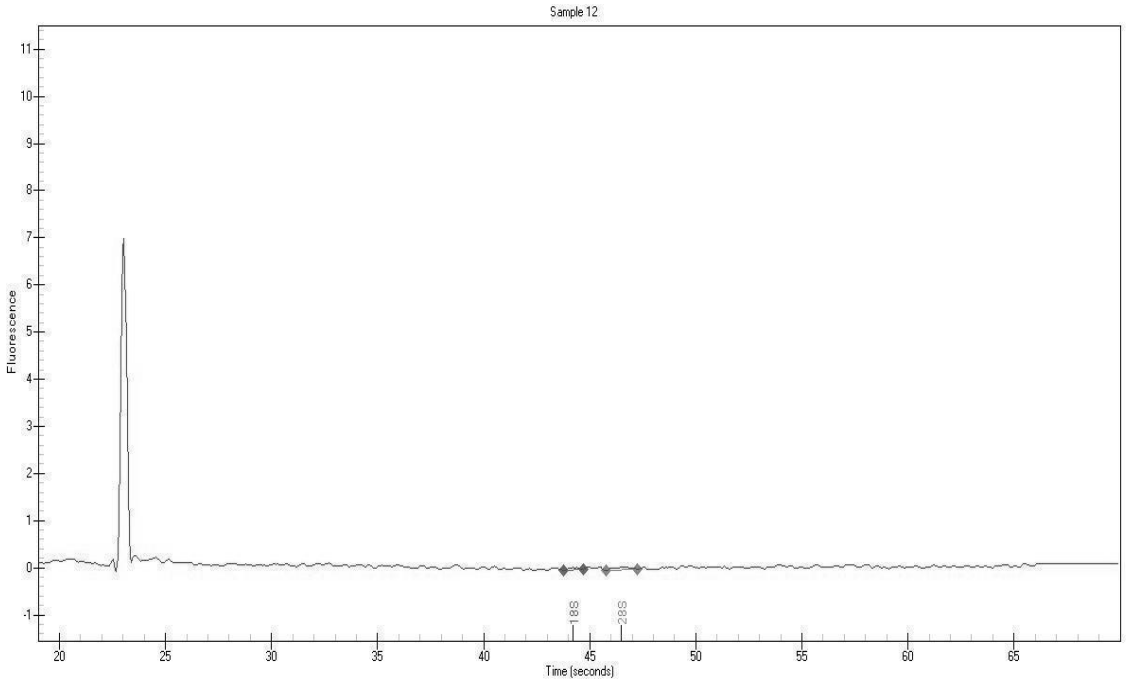

Figures 11C and 11D

The wells above (Figure 11) contained DEPC-treated water which was to ensure that the loading buffer that was added to the other wells with the RNA samples was not contaminated. Assuming the loading buffer was not contaminated, no RNA peaks should be seen on these charts and this holds true for all four wells. Therefore, the fluorescence peaks that appear in the normal and decellularized lung samples will only be derived from the sample itself and not the loading buffer, which allows accurate quantification of RNA content.

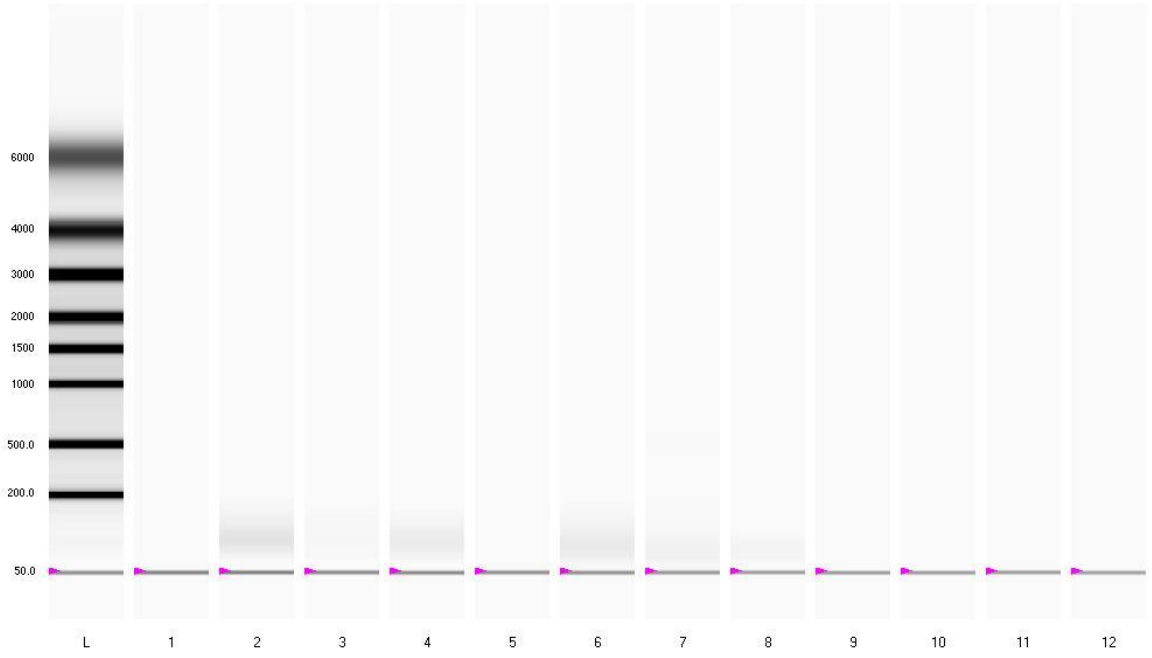

Figure 12: Virtual gel image of RNA from decellularized lungs samples generated by the Experion automated electrophoresis instrument. From left to right: 1-mouse lung 1, 2-pig distal 1, 3-pig small airway 1, 4-pig large airway 1, 5-mouse lung 2, 6-pig distal 2, 7-pig small airway 2, 8-pig large airway 2, 9-12: DEPC-treated water

The virtual gel image created by the instrument (Figure 12) also showed evidence of miRNA presence by the faint bands of about 50-200 nucleotides present in lanes 2 (pig distal), 4 (large airway) and 6 (pig distal of second set). The lower the peak the more smeared the band will look in the image. The DEPC-treated water appeared blank which indicated complete absence of RNA molecules as previously evident from the spectra.

Sample	RNA quality index (2 decimal places)
Normal mouse lung	2.88
Decellularized mouse lung (1st batch)	0.72
Decellularized mouse lung (2nd batch)	0.00
Normal distal pig lung	1.88
Decellularized distal pig lung (1st batch)	0.42
Decellularized distal pig lung (2nd batch)	0.42
Normal pig small airway	0.00
Decellularized pig small airway (1st batch)	0.24
Decellularized pig small airway (2nd batch)	1.42
Normal pig large airway	0.00
Decellularized pig large airway (1st batch)	4.06
Decellularized pig large airway (2nd batch)	3.69
DEPC-treated water (well 9)	0.47
DEPC-treated water (well 10)	0.21
DEPC-treated water (well 11)	0.65
DEPC-treated water (well 12)	2.24

Table 7: RNA quality index (RQI) of normal lung samples from first electrophoresis run and decellularized lung samples and DEPC-treated water wells from second electrophoresis run.

The RNA quality index (RQI) is a value that represents the overall quality of an RNA sample. It uses an algorithm based on many features of the sample spectrum such as the height of the peak for 18S rRNA and the ratio of the rRNA peaks to the total area of the electropherogram. It uses a set of standardized degraded RNA for comparison with the tested samples and uses the algorithm to generate a value between 1(low quality) and 10 (high quality) RNA. RQI numbers were surprisingly low (Table 7) as the previous measurements of RNA concentration and A260/A280 ratios were of acceptable purity for the normal lung and second batch of decellularized lungs. A couple of anomalies were normal mouse lung, and decellularized pig large airway from the 1^{st} and 2^{nd} batches. These were of better RNA quality. It is possible that the RNA degraded during the preparation of the chip for automated gel electrophoresis. The DEPC-treated water also contained ribosomal RNA which is a sign of minimal contamination. In addition, this algorithm for RQI is generally used for cellular RNA samples, as the algorithm is based on the 18S and 28S values. Therefore, we cannot rely on the RQI values since the RNA samples here were isolated from exosomes.

qRT-PCR

The data showed that all the miRNAs were expressed significantly more in normal mouse lung compared to the decellullarized mouse lungs. The same applied to pig distal lungs.

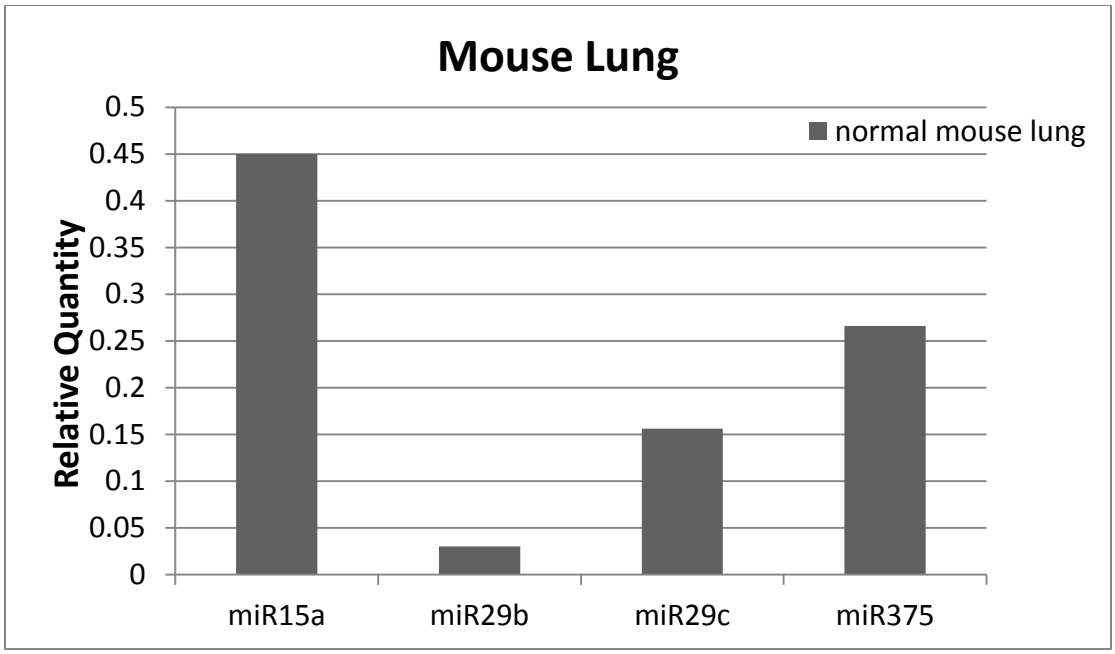

Figure 13: Expression levels of microRNAs in normal mouse lung versus decellularized mouse lung. The average C_t percentage variance for each sample done in quadruplicate tested for each gene was less than 5% (Cumming et al., 2007)

All the results were normalized to pig distal lungs as these had the highest amount of RNA. The software sets the calibrator as '1' which is the maximum relative quantity value. Therefore, assigning the relative quantity as '1' for the sample that had the highest amount of RNA would provide the opportunity to observe the relative expression of all the other samples, which had lower levels of RNA. Figure 13 shows that normal mouse lung mostly expressed miR15a and miR375, with some miR29c and minimal amounts of miR29b. The decellularized mouse lung does not have any microRNA expression, suggesting the absence of exosomes. Profiling for miR375 on all decellularized samples was done separately. Then, the data from this plate was added to the bar charts and displayed along with the other miRNA probes.

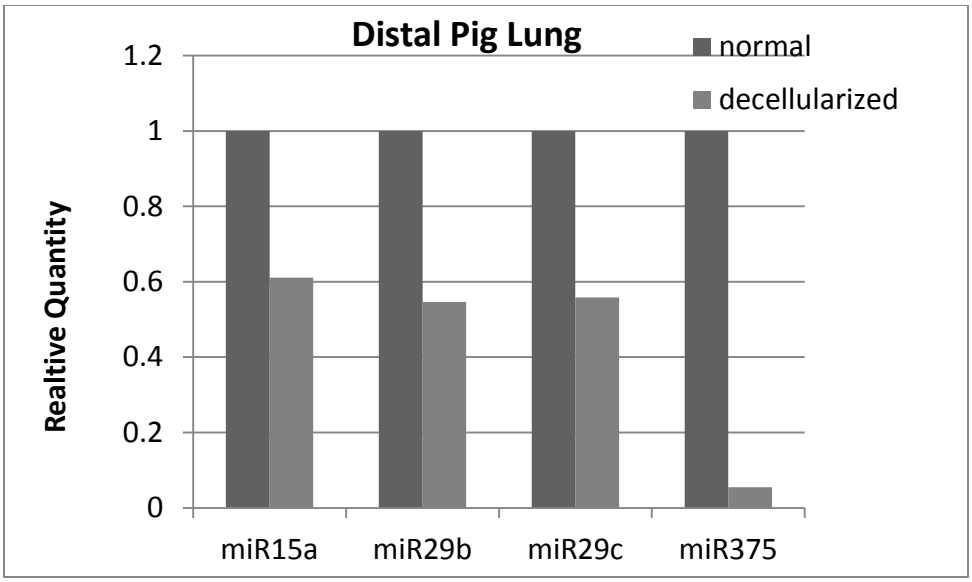

Figure 14: Expression levels of microRNAs in normal versus decellularized distal pig lung. The average C_t percentage variance for each sample done in quadruplicate tested for each gene was less than 5% (Cumming et al., 2007)

As expected, the normal pig distal lung region has much higher miRNA expression than its decellularized counterpart (Figure 14). All three miRNAs miR15a, miR29b and miR29c were still present in decellularized pig distal lung, the highest being miR15a followed by almost equal amounts of miR29b and miR29c.

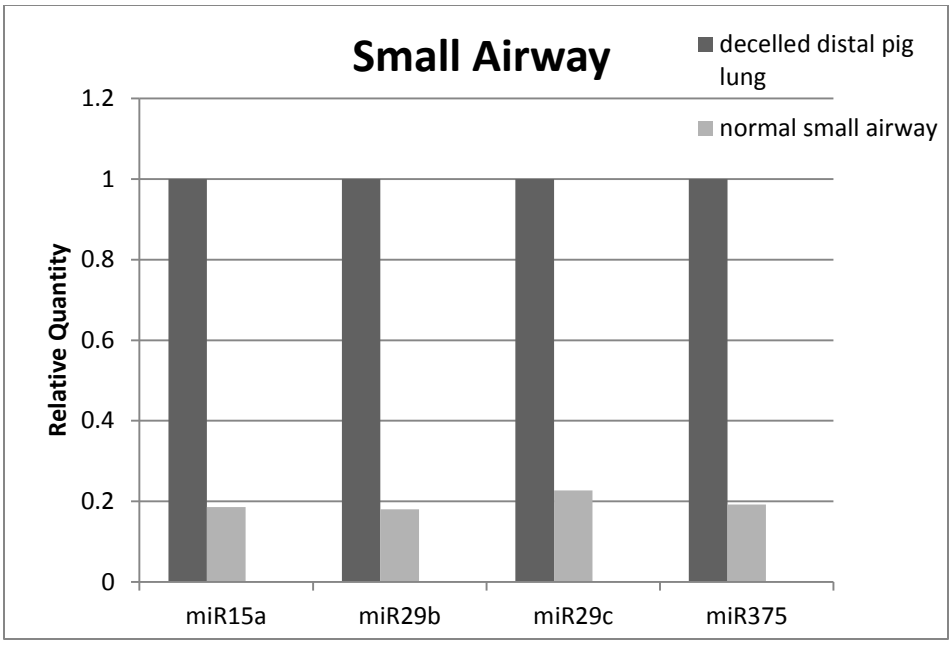

Figure 15: Expression levels of microRNAs in normal pig small airway versus decellularized pig small airway. The average C_t percentage variance for each sample done in quadruplicate tested for each gene was less than 5% (Cumming et al., 2007)

The normal small airway samples overall had less miRNA expression than pig distal lung. Mir29c had the higher expression while the other three had about the same level of expression at a lower relative quantity compared to miR29c. The decellularized small airways had an undetectable amount of RNA (Figure 15). Importantly, all decellularized pig distal lungs had as much as three-fold higher miRNA expression compared to normal small airways. This indicates the many small niches distal lung has which may have trapped the miRNAs despite the decellularization whereas the small airways probably did not due to their simpler, tubular geometry.

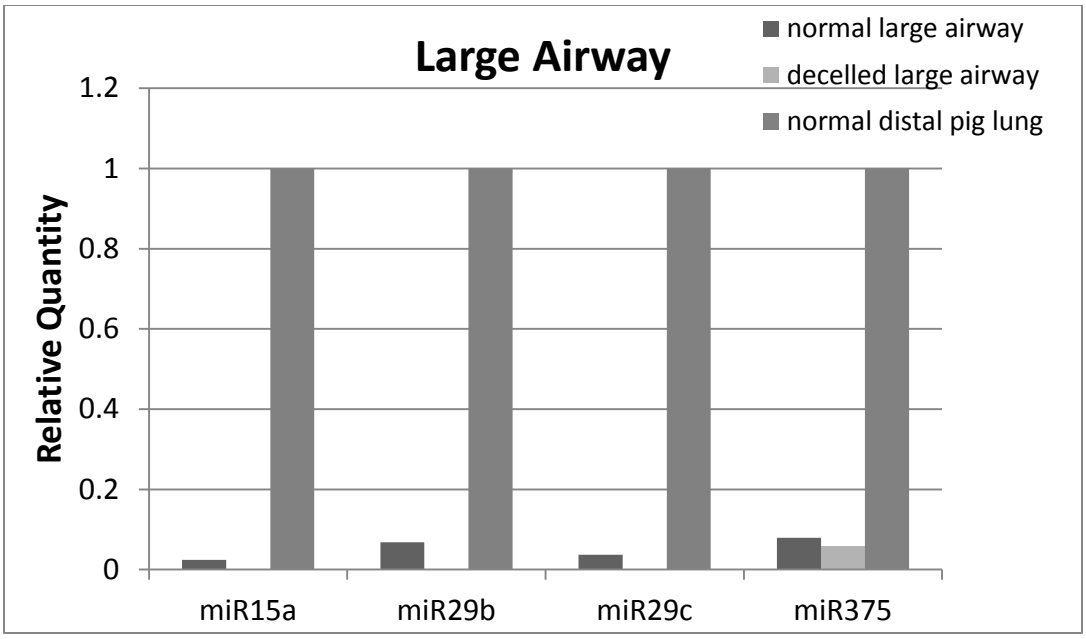

Figure 16: Expression levels of microRNAs in normal pig large airway versus decellularized pig large airway. All samples are normalized to distal pig lung (non-decellularized). The average C_t percentage variance for each sample done in quadruplicate tested for each gene was less than 5% (Cumming et al., 2007)

Normal large airway samples had very low amounts of all miRNAs (Figure 16), even less than the normal small airway samples (Figure 15). This may reflect the effect of the decellularization process on cavities such as the large airway which possibly does not contain a lot of the miRNA probes tested for. As the large airways contain the most cartilage and are relatively distant from the actual lung tissue, they may not contain the miRNAs typically expressed in the distal lung.

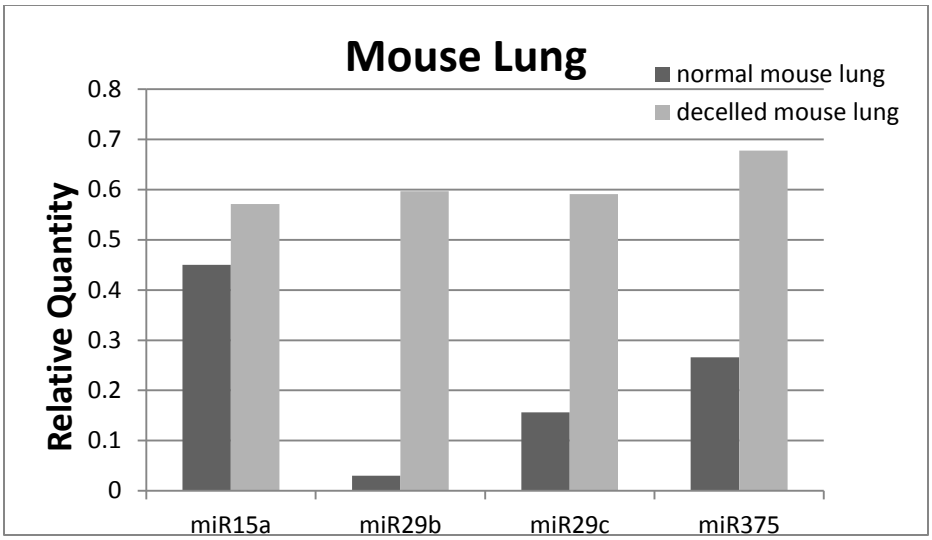

Figure 17: Expression levels of microRNAs in normal mouse lung versus decellularized mouse lung of the second batch. The average C_t percentage variance for each sample done in quadruplicate tested for each gene was less than 5% (Cumming et al., 2007)

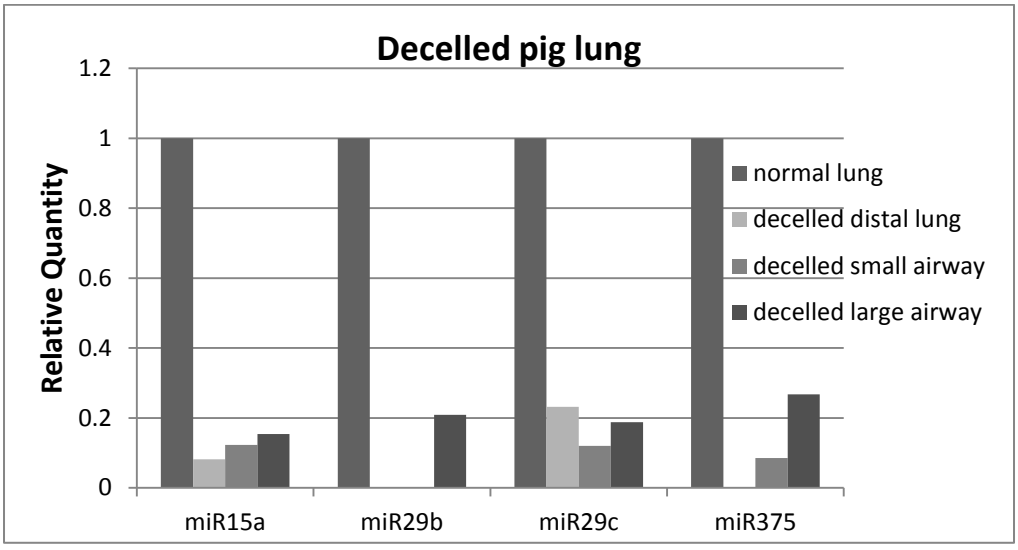

Figure 18: Expression levels of normal pig lung versus decellularized pig lung from the 2nd batch. The average C_t percentage variance for each sample done in quadruplicate tested for each gene was less than 5% (Cumming et al., 2007)

Surprisingly, decellularized mouse lungs from the second batch had higher relative expression of all probes compared to normal mouse lungs (Figure 17). This contradicts the data obtained for the RNA concentrations of these samples (Table 5) and perhaps indicates technical errors during the conversion to cDNA or real-time PCR. Overall, decellularized pig large airway had the highest relative expression for miR15a, miR29b and miR375 (Figure 18) whereas decellularized distal pig lung was the most highly expressed in the first batch of decellularized samples (Figure 14). The only expression was mir29c, which was most highly expressed in decellularized distal pig lung. There was no detectable expression of miR29b in decellularized distal pig lung and decellularized small airway. The heterogeneity in this real-time PCR data may be due to the batches coming from two separate lung tissue sources.

Bradford Assay

The concentrations of protein in the lung samples were calculated using the BSA standard curve. The overall protein concentrations in the normal lung samples were much higher than their decellularized counterparts (Table 8). Among the normal lung samples, mouse lung had the largest amount followed by pig distal, large airway and then small airway. This is the same trend seen in the RNA concentration measurements where the small airway had less RNA than the large airway in normal lungs. However, when it came to decellularized lungs, pig small airway samples had the largest amount of protein with a similar amount in large airway followed by pig distal lung and then mouse lung.

This is in contrast to the RNA concentrations as the decellularized distal pig lung was the highest in that case (Table 6). It can be concluded from the data that a specific RNA concentration in a sample does not have to correlate with the protein concentration from that same sample however for the most part, the RNA and protein concentrations of both normal and decellularized samples seem to have a significant positive correlation (Figure 19).

Sample	**OD595**	**Calculated protein concentration (mg/ml)**
Mouse lung	1.445	2.331
Distal pig lung	1.055	1.476
Pig small airway	0.756	0.821
Pig large airway	0.854	1.036
Decellularized mouse lung	0.527	0.319
Decellularized pig distal lung	0.592	0.461
Decellularized pig small airway	0.634	0.553
Decellularized pig large airway	0.627	0.539

Table 8: Calculated protein concentrations in normal and first set of decellularized lungs

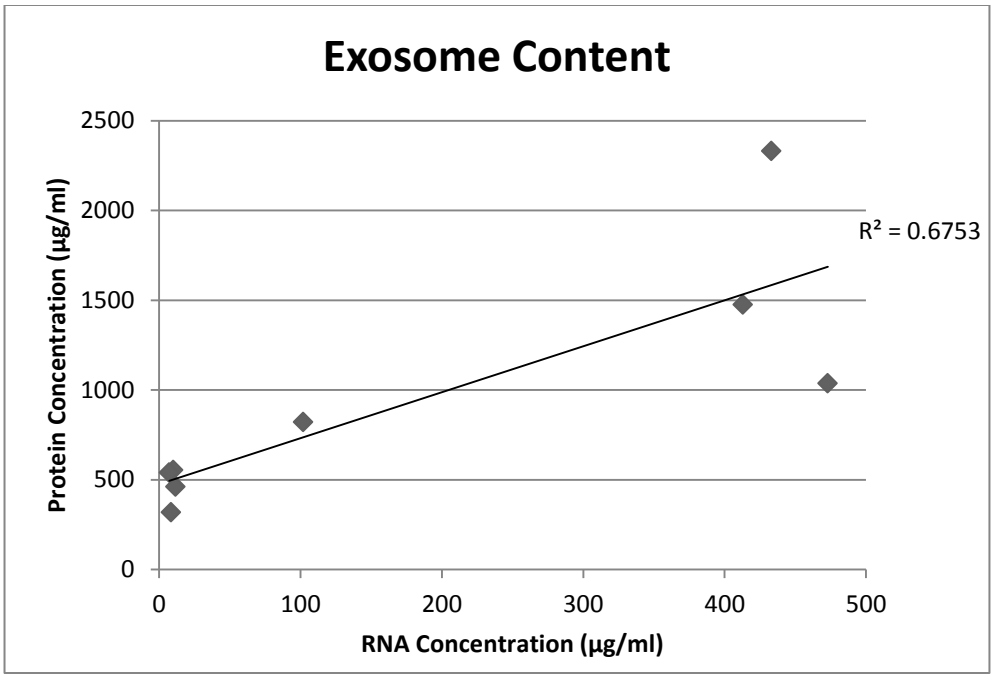

Figure 19: Comparison of observed RNA and protein concentration in exosomes from all samples.

Quantification of exosomes for cell culture

Using the BSA standard curve, the protein concentration of the decellularized distal pig lung exosome sample was calculated using sample without dilution, 1:10 and 1:100 dilutions as shown below in Table 9. However, the OD reading did not go down with dilution indicating a very high amount of protein in the sample. The Bradford assay tends to show high variability, especially in samples with higher protein concentrations (Lu et al., 2010). Nevertheless, the estimated value was significantly high to be used in cell culture, based on previous exosome delivery research (Wahlgreen et al., 2012). In this study by Wahlgreen et al., plasma exosomes were delivered to monocytes and lymphocytes silence a gene responsible for the inflammatory response. The exosome concentration they used was in the range 0.25-1µg/µl and their dose-response experiments showed that about 500µg of exosomes were necessary to completely silence the gene. Therefore, I postulated that this figure would be my threshold exosome concentration to go by and since I observed 0.772µg/µl in my sample without dilution, I went by this concentration. My sample volume was 1.5ml which meant that it contained the required amount of exosomes.

Sample	**OD595**	**Protein concentration (mg/ml)**
No dilution	0.760	0.772
1:10	0.789	8.419
1:100	0.767	78.9

Table 9: Estimated protein concentrations of exosomes from decellularized pig distal lung

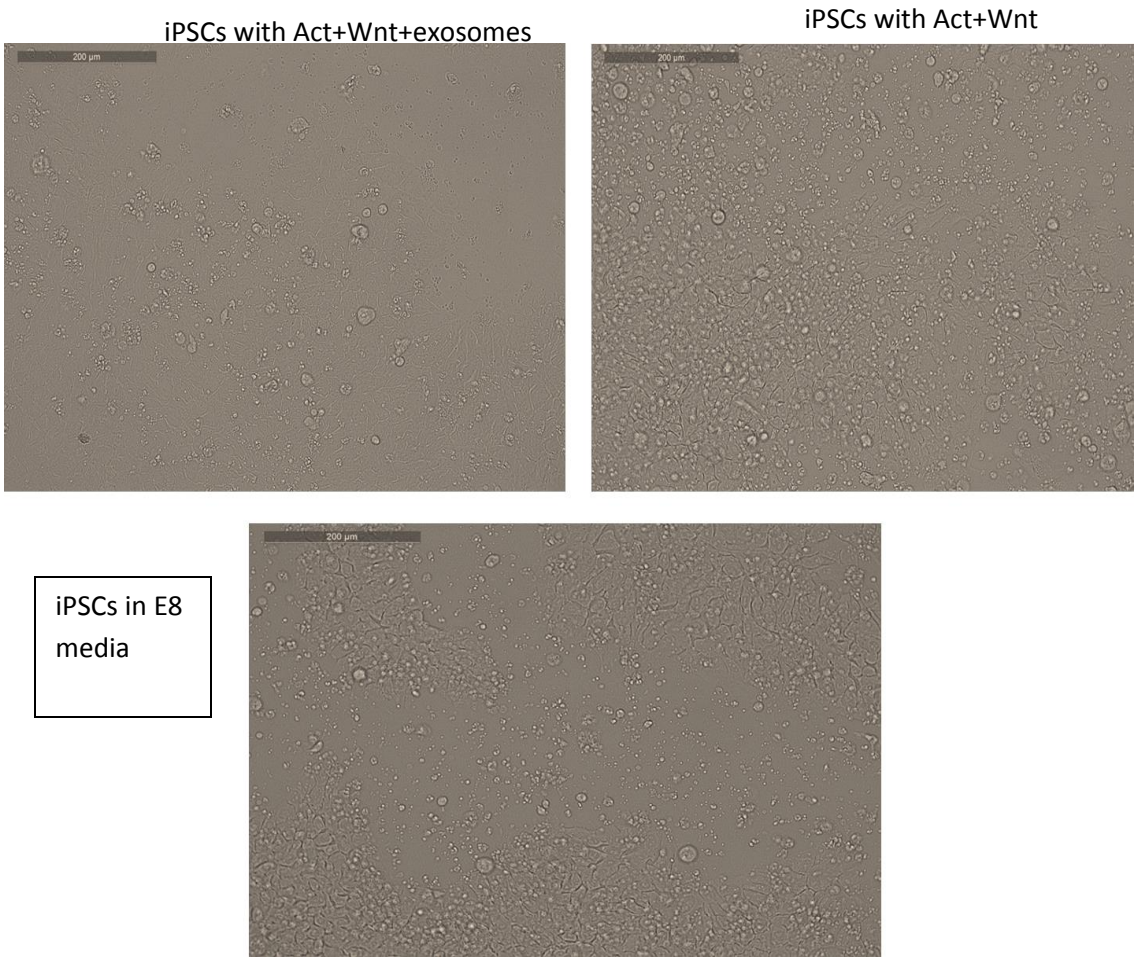

Figure 20: Brightfield images of iPSCs at day 0 of differentiation to definitive endoderm. A-iPSCs with Act, Wnt and exosomes from decellularized distal pig lung, B-iPSCs with Act and Wnt and C-just iPSCs in E8 medium. The scale bar is 200µm.

At day 0 of differentiation, iPSCs from all wells appeared similar in morphology and size, and were quite dispersed across the plate. Individual colonies could be easily visualized. The exosomes from decellularized distal pig lung were added on to the first two groups of iPSCs on day 2.5. The appearances of the cells at this point were not much different to the ones at day 0 of differentiation. Even the wells to which only Activin and

Wnt were added did not show any significant difference in cell morphology and distribution. By day 6, the wells with the exosomes added exhibited different morphology compared to the wells to which only activin and wnt were added (Figure 21) as demonstrated by the clumps that the cells formed (Figure 21A). The wells to which nothing was added preserved the typical round morphology of iPSCs, as expected (Figure 21C).

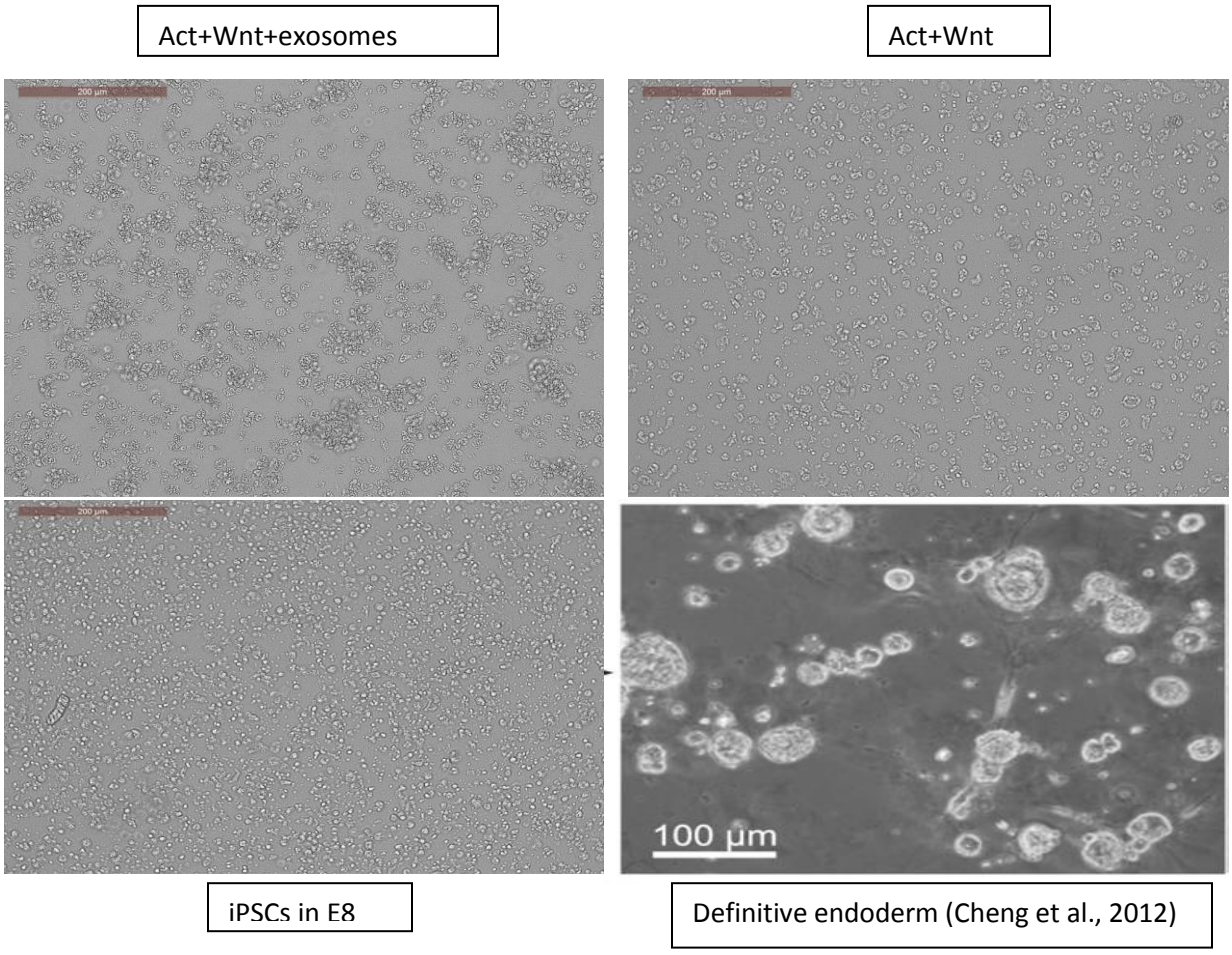

Act, Wnt and exosomes from decellularized distal pig lung, B-iPSCs with Act and Wnt, C- iPSCs in E8 medium and D- the appearance of definitive endoderm cells (Cheng et al. 2012). The scale bar is 200µm for A,B, and C and 100µm for D.

RNA isolated from these cell cultures were of high quality and are shown in Table 10.

Day	**RNA concentration (µg/ml)**	**A260/A280**
day 0 iPSCs	31.4	2.257
day 6 no exosomes	7.952	2.000
day 6 with exosomes	3.181	2.100

Table 10: RNA analysis during iPSC differentiation to definitive endoderm

Automated gel electrophoresis

Although most samples had detectable amounts of RNA by spectrophotometry, the Bioanalyzer could not detect any amount of miRNA. The device can detect as low as 5ng of RNA per 1µl sample. Only the day 6 sample not treated with exosomes produced a detectable peak which was not in the miRNA region (Figure 22A). It suggests the presence of mRNA in this sample. In contrast, the day 6 sample that was treated with exosomes showed no peaks at all (Figure 22B) which is not surprising as the RNA concentration (Table 10) was below the detectable amount of the Bioanalyzer. Cell culture samples with undifferentiated iPSCs grown on E8 did not give a high yield of RNA. This can be attributed to poor RNA isolation technique.

qRT-PCR for cell culture samples at day 6 showed no detectable expression of mature lung or definitive endoderm markers (Figure 23). Surprisingly, Oct4 was still detected in the cells that were culture with exosomes, indicating some retension of pluripotency. However this is only one marker and it is not enough to say that these cells remained as iPSCs since their morphology had drastically changed (Figure 21).

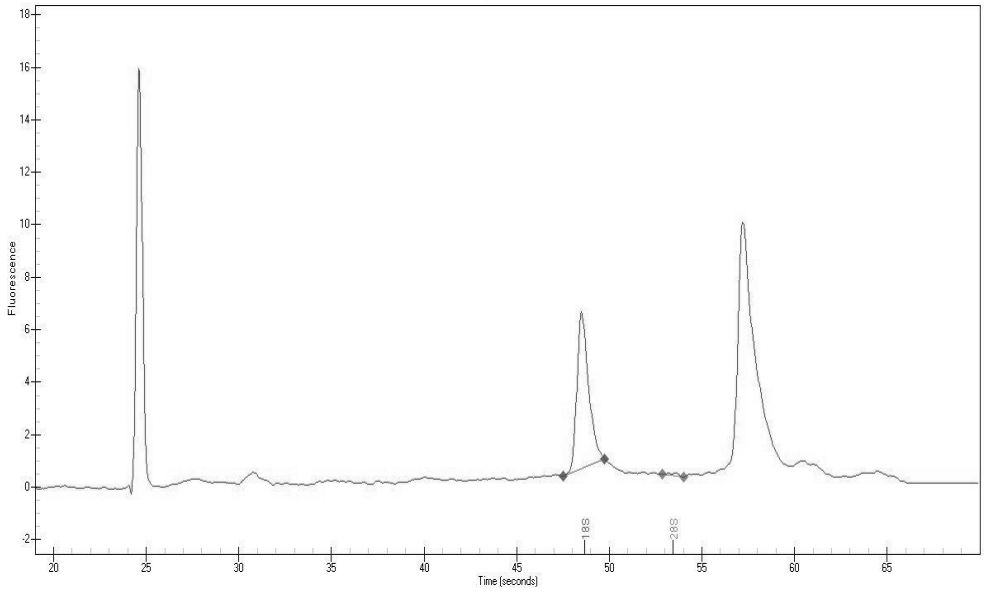

Figure 22A: Day 6 iPSC culture to definitive endoderm without exosomes

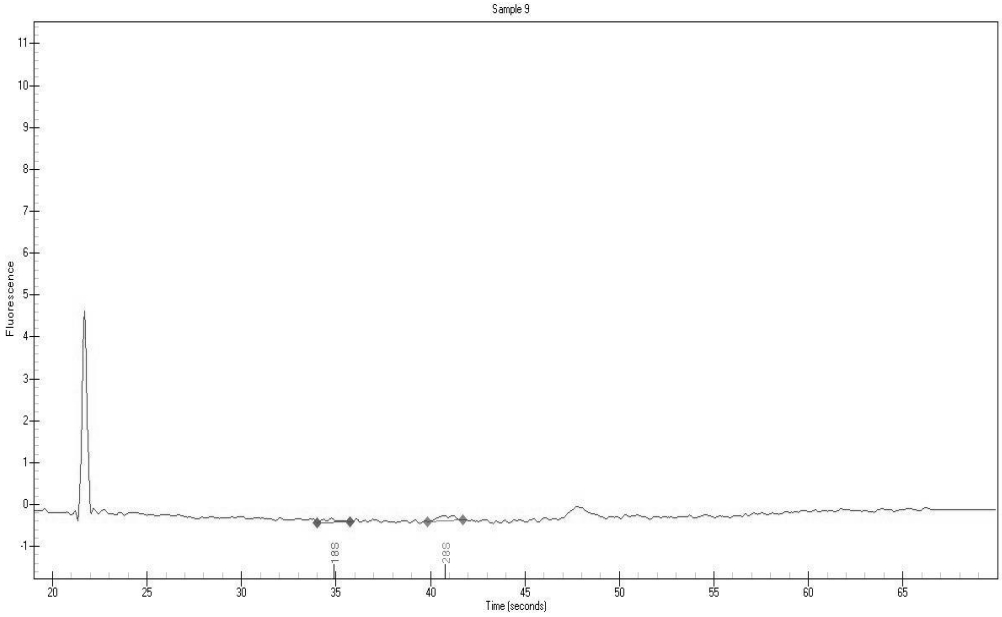

Figure 22B: Day 6 iPSC culture to definitive endoderm with exosomes

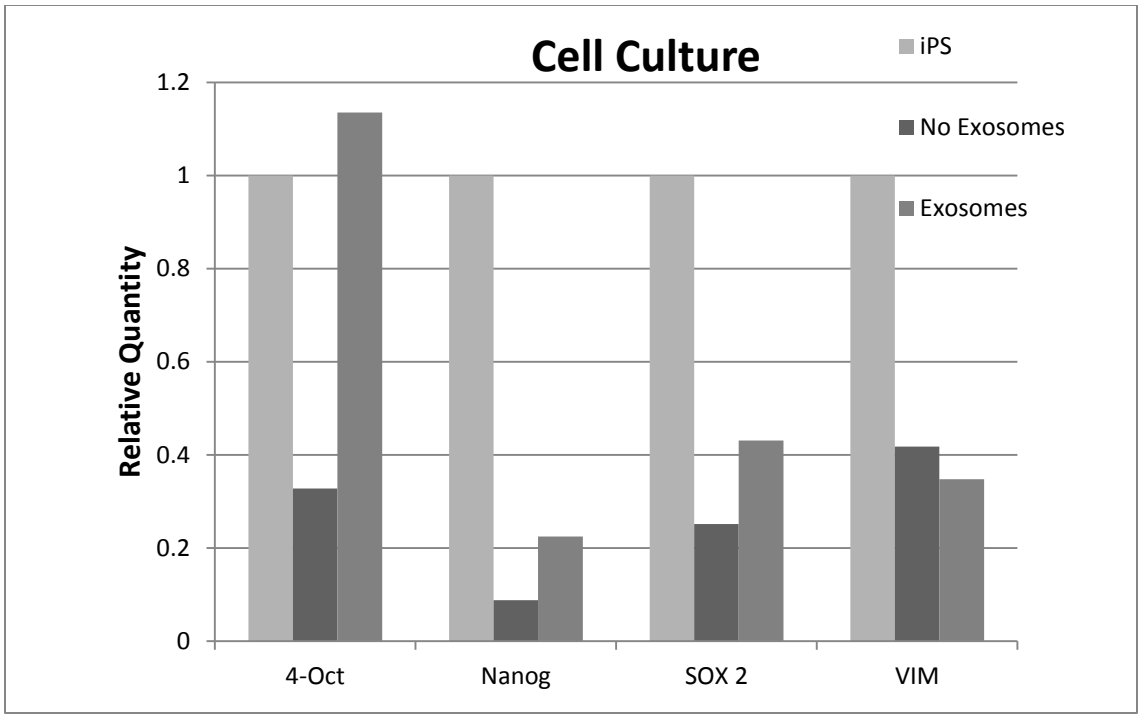

Figure 23: qRT-PCR data for samples from iPSC culture to definitive endoderm. All iPSC samples were pooled together and are from day 0. The samples with and without exosomes are from day 6 of differentiation. The data percentage variance for each sample done in quadruplicate tested for each gene was less than 5%

Discussion

The need for a suitable scale-up method for translational therapy was deemed necessary by the huge number of cells required for recellularization of large essential organs. Reaching a number in the order of billions with 2D cell culture is very time-consuming and costly as many plates and space is needed. Therefore, iPSCs were cultured in stirred-flask bioreactors and the cells observed for 6 days. Even though the conditions were set similar to the 2D culture conditions, iPSCs were depleted in a mere 24 hours. The possibilities were determined by metabolite analysis and cell counts. The lactate assay showed evidence of significant cell death from day 0 to day 1. Lactate levels increased to about 11ng/µl and then plummeted down to 3ng/µl on day 2. The increase from day 0 to day 1 could be attributed to the lactate released from the cells during death. Afterwards, the lactate levels would decrease as the media was changed every 2 days. Therefore, on day 2, there was much less lactate as there were no cells to produce any more of it. Lactate levels gradually decreased after day 2 with each media change but nothing in comparison to the first drop as most cell death had already taken place and the slow decrease in lactate is due to each consecutive media change. The typical lactate level for iPS cells in culture is around 2µM (Varum et al., 2011). The level reached in the bioreactor is about 0.12 ng/µl which is equivalent to 0.12µM. The iPSCs did not even reach the lactate levels expected therefore it is likely that a lot of cell death occurred even before day 1 was over so that some metabolism took place but could not proceed due to cell depletion.

The glucose assay showed an initial level of glucose that is much lower than the characteristic glucose concentration in serum-free media such as mTESR1, just after the cells were transferred to the bioreactor. mTESR™1 medium is known to contain about 2.466 mg/ml glucose so this value was too low. This may be attributed to the fact that cells were under stress because they had already been growing in mTESR1 on the plates. The glucose value had increased significantly by day 2. This is inaccurate since cells are unable to produce glucose and it is important to state that is higher than the glucose concentration of mTESR1 itself. It is said that pluripotent stem cell types such as iPSCs and ESCs use anaerobic glycolysis as their major metabolic pathway (Madonna et al. 2013). This is due to the hypoxic conditions that stem cells normally encounter in the niche and is their natural metabolism. As oxygen levels were low in the bioreactor, it is likely the cells were responding to this by carrying out glycolysis, which explains the low glucose and high lactate levels observed on day 4. Glycolysis splits a glucose molecule into two pyruvate molecules which does not require oxygen therefore glucose levels will be high in the initial days of iPSC culture, such as day 2. As the cells adapt to the hypoxic conditions, they start using glucose for aerobic respiration which may also be the reason for the decrease in glucose on day 4.

The initial decrease in cell number is what is expected in the transition process from 2D to 3D culture. The cells need the time to adjust to low oxygen levels. This explains the recovery at day 4. The subsequent continuous decrease in cell number until complete depletion may be due to lack of an appropriate matrix to support cell attachment. Even though the ROCK inhibitor was used in these cultures, it was not able to compensate for the lack of a matrix (Chen et al., 2013). It is also possible that the bleach used to clean the

apparatus after each experiment could have remained in the crevices of the bioreactor lid. This may have caused the sudden cell death observed in many other trials of this 3D cell culture. Perhaps a supporting matrix such as collagen-coated beads would be a suitable alternative for future experiments.

The ROCK inhibitor is said to increase embryonic stem cell (ESC) survival by attenuating dissociation-induced apoptosis (Watanabe et. al 2007). Further work has shown that this survival-promoting effect is evident in the first half-day of cell culture as no changes were observed in subsequent days of cell culture (Watanabe et al. 2007). For this reason, the ROCK inhibitor was added to the bioreactor culture in the hope that it would improve iPSC survival during the transfer from the six-well plates to the stirred-flask bioreactor. The effect of the molecule was also tested in serum-free culture and the results showed that it made no difference to cell survival (Watanabe et al. 2007). In addition, the ROCK inhibitor does not affect ESC differentiation in suspension culture (Watanabe et al., 2007), which opens the possibility of utilizing this molecule in iPSC differentiation to endoderm. Although that particular study (Watanabe et al., 2007) focused on ESC culture, other studies have demonstrated the effectiveness of this molecule in iPSC suspension culture as well (Larijani et al., 2011, Shafa et al, Olmer et al. 2012, Kehoe et al. 2010). It is important to mention the potential of the ROCK inhibitor not only in pluripotent cell culture but also in other cell cultures such as the many cell types of the lung. Indeed, airway epithelial cell proliferation is improved by addition of ROCK inhibitor but not their differentiation to mucous or ciliated cells (Horani et al. 2013). The implications of this study are that the ROCK inhibitor could be utilized in maintenance of endoderm progenitor cells. There are many conditions in 3D

suspension culture that could have caused the massive cell death observed here. The oxygen and carbon dioxide levels were at standard levels used in pluripotent stem cell culture as were the incubator temperature and humidity. The possibility that the lack of some sort of support or platform for the cells was the cause of death may be the answer. However, this cannot be the sole reason as many studies have been successful in iPSC serum-free suspension culture without any matrix support (Larijani et al., 2011, Shafa et al, Olmer et al. 2012, Kehoe et al. 2010). Microcarriers are a very suitable matrix for pluripotent stem cell culture in suspension as they give the cell the support they need during the transition from the plates to the bioreactor. The conventional method is to coat these microcarriers with extracellular matrix material such as Matrigel. Many ECM materials come from animal sources, which would ideally not be a translatable clinical therapy. One such study linked the benefits of the ROCK inhibitor with microcarriers by culturing the cells with ROCK on microcarriers with and without ECM coating (Chen et al. 2013). The end result was that ROCK was able to replace the role of the ECM coating by promoting cell survival (Chen et al. 2013). It is a desirable alternative to culturing cells with animal matrices such as Matrigel.

Exosomes

RNA concentration measurements in exosome preparations indicated variability in RNA quality. Abnormally high concentrations of RNA with a low A260/A280 ratio are usually due to the presence of contaminants such as proteins. The differences in RNA concentration could be attributed to technical inexperience since the quality improved as more samples were processed.

Automated RNA electrophoresis

Normal lung samples gave very tall, sharp peaks of similar size, regardless of species. This indicates that miRNAs among species must be similar in structure to produce fluorescence peaks at the exact same time. The typical miRNA region on these spectra is said to be between 10 and 40 seconds (Becker et al 2010). All of the peaks for normal lungs appear within this region which confirms the presence of miRNAs. This is the result typically expected of normal lungs as they contain cells and therefore many exosomes in the intracellular and extracellular environment. The mouse, pig distal and small airway samples also had a smaller hump appear right after the prominent, large peak which is still within the miRNA region. These may be longer miRNA sequences as the larger the molecular weight, the later they will appear in the spectra. These smaller humps did not appear in the normal large airway spectrum. Any sharp, prominent peaks after 40 seconds would typically represent tRNAs if between 50 and 80 seconds and small rRNAs if between 80 and 150 seconds. None of the spectra for normal lung samples displayed these features. The main RNA component of exosomes is miRNA so it is an indication of good exosome isolation to only see miRNA even though this miRNA may not only be from the exosomes themselves. It is also possible that there may be residual miRNA or fragmented mRNA from the tissue. When mRNA is degraded it will have shorter sequences so the instrument will detect this as short sequence RNA which will appear in the miRNA region. Therefore, the small humps mentioned earlier may be some degraded mRNA leftover from the exosome isolation process. As a result, the instrument may overestimate the amount of miRNA and this method of automated gel electrophoresis may only be accurate for RNA samples of very high quality. Although the

RNA from these normal lung samples were of very high quality, a part of the miRNA region will represent a number of undefined small RNA fragments and this is unavoidable as it is expected to have a minimal amount of RNA degradation during RNA isolation and loading of the chip for electrophoresis. Current methods cannot guarantee isolation of pure miRNA. The only way to identify miRNA is to proceed to real-time RT-PCR using assays for several miRNAs that are expected to be in the samples. All eukaryotic cells possess ribosomal RNAs 18S and 28S that typically appear as very tall and sharp peaks at 43 and 49 seconds respectively. Both of these components were absent from the spectra in all normal lung exosome samples. This is another good feature of successful exosome isolation as no cells should remain after the process and hence no ribosomal RNA. The RNA quality index measures the amount of 28S ribosomal RNA to the amount of 18S ribosomal RNA to generate a ratio as means to determine RNA quality. The 28S rRNA degrades much more quickly than the 18S rRNA so a ratio of 10 would indicate high quality RNA with minimal degradation. However, this ratio can only be generated in cellular RNA samples as exosomes do not contain ribosomal RNA. Nevertheless, most of the exosomal RNA samples had an RQI, albeit at low values. The anomalies, normal mouse lung and decellularized pig large airway from batch 2, possibly did not undergo successful exosome isolation or were contaminated during the RNA isolation or well loading procedures. Even the wells with DEPC-treated water had an RQI which could explain the RQI of the lung samples although it could be a combination of contamination of the DEPC-treated water and contamination of the sample with cellular i.e. ribosomal RNA. It is also possible that the automated electrophoresis machine is contaminated. The only way to overcome this would be to carry out the ‘deep clean’

procedure by cleaning the electrodes in the machine with probe wipes. Even though the routine cleaning before and after every experiment reduces the chances of contamination, the ‘deep clean’ procedure should be carried out after extended use.

The first set of decellularized lungs displayed no signs of rRNA either which also implies successful exosome isolation for these samples. The decellularized mouse lung gave no indication of any type of RNA despite the 8.748µg/ml that appeared in the Implen Nanophotometer. This may be due to the poor A260/A280 ratio which gave a false high of RNA amount. The same applied for the decellularized mouse lung from the second set. This correlates with real-time RT-PCR results since no relative expression of any of the Taqman probes tested was found. Decellularized distal pig lung samples showed a significant amount of RNA. The higher peak in the former may be due to an overestimation of RNA as the RNA isolated from the first set of decellularized samples was not very pure. In contrast, the second set was reasonably pure which is evident from the higher A260/A280 ratio. The decellularized pig small airway showed a higher peak in the second batch compared to the first. In this case, a higher peak may have appeared in the second set as the RNA was more pure and may have been underestimated in the first set. DEPC-water samples did not have any peaks except for the lower marker. This confirms the fact that the DEPC-treated water used in the wells with the samples was indeed not contaminated. The virtual gels generated by the instrument accurately displayed the approximate RNA molecular weight range and purity. Some faint bands were seen that were too high for the miRNA region, which appears between 200-500 nucleotides. This, again, may indicate the presence of degraded RNA which is displayed in the spectrum as a large peak in the miRNA region. As this is the first of decellularized

lungs the results do not have to be depended on, as the RNA purity was low in this case. The second set of decellularized lung samples give a much more accurate and precise estimation of miRNA content as their RNA was very pure. It is not to say that decellularized pig distal lung did not contain miRNA but rather that the amount is overestimated in the first set. Furthermore, the first electrophoresis experiment results cannot be completely relied on as the decellularized mouse, pig small airway and large airway samples showed peaks reduced to negative fluorescence units which is possibly due to pipetting errors while the wells were being filled with sample. This was improved when the samples were run a second time when smaller peaks appeared which accurately demonstrated miRNA content. Therefore, it is safe to say that all normal lung and decellularized pig distal lung samples had significant amounts of RNA.

qRT-PCR data showed that normal mouse lung expressed all tested miRNA with miR15a being the highest, followed by miR375, miR29b and a minimal amount of miR29c. MiR15a was significant because it had a relative quantity of 0.45 which means it expressed 45% of the amount of normal pig distal lung. MiRNAs are subjects of recent research so many of them have unknown or not clear-cut functions. Most studies have focused on the effects of their deletion or overexpression. miR15a is said to be involved in cell cycle control and apoptosis (Bandi et al. 2010). Their deletion has been associated with the increase in cyclin D1 which results in hyperproliferation of cells in the lung leading to adenocarcinomas and squamous cell carcinomas.

The miR29 family of miRNAs are normally expressed in lungs of adult pig and mouse, specifically in the alveolar wall and pleura and in mesenchymal cells at entrance of the

alveolar duct (Cushing et al., 2011). In regards to qRT-PCR data, the relative quantity of miR29b was quite low for normal mouse lung compared to miR29c. It could be that miR29b is normally expressed at low levels in normal adult mouse lung to maintain essential cellular processes but is still fundamental for proper lung function. Cushing et al. also studied changes in miR29 levels over the course of mouse development. MiR29 levels gradually increased from as early as the embryonic stage, becoming the highest in adult lung. This stresses the importance of miR29 in development and suggests a role in alveolar development. MiR29 levels could be a useful determinant of stem cell differentiation stage in the developing lung. As stated previously, the functions of miRNAs are mainly determined by observation after deletion or exploring their therapeutic potential through overexpression or exogenous delivery. Downregulation of miR29 is observed in pulmonary fibrosis models (Cushing et al 2011) and is associated with up-regulation of pro-fibrotic target genes. Moreover, the expression levels of miR29 decreased with the severity of the disease and the pro-fibrotic genes increased. It can be seen that the miR29 family is essential for maintenance of normal lung structure by regulating ECM deposition and remodeling.

MiRNAs also play a critical role in cell signaling mechanisms. For instance, it was found that the miR29 family of miRNAs are downstream targets of the TGF-β-Smad3 signaling pathway. As many ECM proteins are target genes of miR29, it is highly associated with the fibrosis of many organs such as lung , liver and heart. Indeed, studies on bleomycin-induced Smad3 knockout mice versus bleomycin-induced wild type mice have shown that the downregulation of miR29, along with the emergence of fibrosis is Smad3-dependent (Xiao et al. 2012). This demonstrates the importance of miRNAs in essential

cell processes and their potential future role in cell therapy. The same study used ectopic expression of miR29b to improve the condition of bleomycin-induced pulmonary fibrosis in mice by blocking progressive fibrosis. Fibrosis is caused by activation of fibroblasts in the lung that thicken around the alveoli and cause scarring and is caused by many environmental factors such as asbestos. Therefore, the existence of miR29b and miR29c in the decellularized mouse lung would be advantageous when iPSCs or endodermal progenitor cells are injected into the lung because they would prevent potential fibrosis if a particular patient is prone to these fibrotic factors. This goes back to the concept of the preservation of the ECM in decellularized matrices and the molecular cues needed for correct regeneration.

Mir375 was expressed 0.3 times the quantity of normal pig distal lung. Pigs have much larger lungs therefore decellularization would be more challenging compared to mouse lungs, especially the distal parts of the lung. Therefore, it is not a surprise that a significant amount of miR375 remained in decellularized distal pig lung as opposed to none in the decellularized mouse lung. Mir375 expression starts to increase upon differentiation to definitive endoderm and then gradually decreases upon further differentiation to pulmonary or hepatic cells (Wei et al. 2013). In that particular study, embryonic stem cells were differentiated to insulin-producing cells via differentiation to definitive endoderm first. The results showed increased expression of miR375 upon formation of definitive endoderm and started decreasing once the pancreatic progenitors were formed. This demonstrates the significance of miR375 as a good marker of definitive endoderm. Even though slightly more mature cells such as pancreatic progenitors express this miRNA, it will be useful when checking for definitive endoderm

cells during differentiation to pulmonary epithelial cells. Indeed, it is known that miR375 regulates alveolar epithelial cell (AEC) transdifferentiation (Wang et al, 2013). During lung injury, type II pneumocytes trans-differentiate to type I pneumocytes to maintain essential lung functions as type I pneumocytes regulate gas exchange and fluid transport. MiR375 expression gradually decreases during AEC trans-differentiation and is enriched in type II pneumocytes (Wang et al. 2013). Over-expression of miR375 resulted in inhibition of AEC transdifferentiation. This may explain the detection of miR375 in normal mouse lung. It is still a surprise to discover the important role miR375 has in the developing and injured lung because it is firmly established that this miRNA determines islet development in the pancreas (Li, 2014). This is probably due to the fact that miR375 is highly conserved among many species and was first cloned from a pancreatic cell line. The link between miR375 and the lung is fairly new so its various roles are yet to be determined. As mentioned above, miR375 is expressed early in development. As its levels are high at the definitive endoderm stage, miR375 has an even broader set of functions than first thought. This would be useful from our perspective as this miRNA could be used to direct the differentiation of iPSCs or endodermal progenitor cells that are injected into the decellularized lung. Stem cell differentiation to various progeny occurs via inactivation of transcriptional repressors. It is these repressors that keep stem cells in their pluripotent state. One of the ways these repressors can get inactivated is by miRNA silencing, leading the way to differentiation. It was also mentioned in the introduction that differential expression of miRNAs are implicated in several types of cancer. Levels of miR375 tend to decrease in cells affected by non-small-cell lung cancer, suggesting a tumor suppressor function for this miRNA (Yu et al, 2014).

Therefore, not only will miRNAs be used as indicators of development and regeneration, but also as disease markers.

MiR15a is robustly expressed in both adult pig and mouse lungs. The precise role of miR15a in lung development is unknown however functions have been speculated from its down-regulation in non-small-cell lung cancer (Bandi et al., 2009). In this particular disease, cyclin D1 is upregulated and seems to correlate with the down-regulation of miR15a, suggesting it to be a likely target of this miRNA. It was demonstrated that miR15a induced cell-cycle arrest and non-small-cell lung cancer cells escape this cell cycle arrest because miR15a is down-regulated (Bandi et al., 2009). In terms of lung development and regeneration, it could be stated that all healthy adult pig and mouse lungs should have more than a detectable amount of miR15a expression. This is obvious in the qRT-PCR results for normal mouse lung which is expected as total lung was used. It is also evident in the normal pig distal lung, small airway and to a much smaller degree in the large airway. Perhaps miR15a is expressed in the squamous tissue of the lung itself rather than the harder cartilage of the airway.

iPSC differentiation to definitive endoderm

The iPSCs treated with Activin and Wnt appeared very similar to the iPSCs maintained in Essential 8 medium. Many protocols have been created for the differentiation to definitive endoderm which utilize Activin, Wnt and many other factors such as basal fibroblast growth factor (bFGF). According to the results above, this does not hold true for the iPSCs used in this experiment. Every iPSC line retains epigenetic memory from the type of cell it was reprogrammed from (Kim et al., 2010). Therefore, each line is

unique and can behave differently because the chromatin structure in the iPSC nucleus varies in structure and organization. The transcription factors used in the differentiation protocol will interact with the DNA in the iPSCs in an independent fashion in each cell line. This could be a reason for not obtaining definitive endoderm cells. In addition, it is said that miRNAs contribute to iPSCs-somatic donor memory (Vitaloni et al., 2013).This was analyzed in iPSCs derived from cord blood which were compared to hematopoietic progenitor cells (HPCs) differentiated from these iPSCs. MiRNA microarrays were done for both from low-passage iPSCs and high-passage iPSCs derived from HPCs in the cord blood. Interestingly, the low-passage iPSCs retained miRNA expression characteristic of HPCs in comparison to their high-passage counterparts. The iPSCs obtained for this cell culture experiment had been re-programmed from bone marrow fibroblasts therefore it is only logical that these cells retain epigenetic and possibly miRNA memory. According to Vitaloni et al., iPSCs would be considered low-passage if they had undergone 10 passages or less however the iPSCs used in this experiment were passage 14. There is no clear-cut borderline for these characteristics so it is enough to consider the possibility that these iPSCs had memory of their bone marrow origin. If this were true, the epigenetic and miRNA memories of these iPSCs may be a barrier to their differentiation to definitive endoderm.

In stark contrast, the iPSCs that received exosomes from decellularized pig distal lung as well as Activin and Wnt exhibited completely different morphology. They appeared to form clusters of cells, some of them being ring-shaped. This is indicative of definitive endoderm but cannot be confirmed without information from real-time PCR data.

In conclusion, exosomes were shown to remain in pig and mouse lungs, even after decellularization. They contain significant amounts of miRNA that can be used to alter the course of iPSC differentiation to definitive endoderm. Even though large-scale culture was not successful, this method still has great potential in generating large numbers of cells for recellularization. This may help the recellularization process of the pig lung in the long run. It may also be translatable to the clinic when the correct number and types of cells have been generated and successfully reconstitute decellularized pig lung matrix.

BIBLIOGRAPHY

Abbasalizadeh S, Larijani MR, Samadian A, Baharvand H., *Bioprocess development for mass production of size-controlled human pluripotent stem cell aggregates in stirred suspension bioreactor,* Tissue Eng Part C Methods. 2012 Nov;18(11):831-51.

Amit M, Laevsky I, Miropolsky Y, Shariki K, Peri M, Itskovitz-Eldor J., *Dynamic suspension culture for scalable expansion of undifferentiated human pluripotent stem cells.,* Nat Protoc. 2011 May;6(5):572-9.

Bandi N1, Zbinden S, Gugger M, Arnold M, Kocher V, Hasan L, Kappeler A, Brunner T, Vassella E., *miR-15a and miR-16 are implicated in cell cycle regulation in a Rb-dependent manner and are frequently deleted or down-regulated in non-small cell lung cancer.,* Cancer Res. 2009 Jul 1;69(13):5553-9

Becker C, Hammerle-Fickinger A, Riedmaier I, Pfaffl MW., *mRNA and microRNA quality control for RT-qPCR analysis.,* Methods. 2010 Apr;50(4):237-43

Bonvillain RW, Danchuk S, Sullivan DE, Betancourt AM, Semon JA, Eagle ME, Mayeux JP, Gregory AN, Wang G, Townley IK, Borg ZD, Weiss DJ, Bunnell BA, *A nonhuman primate model of lung regeneration: detergent-mediated decellularization and initial in vitro recellularization with mesenchymal stem cells,* Tissue Eng Part A. 2012 Dec;18(23-24):2437-52

Bosman, F.T. and Stamenkovic, I., *Functional structure and composition of the extracellular matrix.,* (2003), J Pathol. 200, 423-428

Chen AK, Chen X, Lim YM, Reuveny S, Oh SK., *Inhibition of ROCK-Myosin II Signaling Pathway Enables Culturing of Human Pluripotent Stem Cells on Microcarriers Without Extracellular Matrix Coating,* Tissue Eng Part C Methods. 2014 Mar;20(3):227-38

Cheng X, Ying L, Lu L, Galvão AM, Mills JA, Lin HC, Kotton DN, Shen SS, Nostro MC, Choi JK, Weiss MJ, French DL, Gadue P., *Self-renewing endodermal progenitor lines generated from human pluripotent stem cells,* Cell Stem Cell. 2012 Apr 6;10(4):371-84

Cumming G, Fidler F, Vaux DL., *Error bars in experimental biology,* J Cell Biol. 2007 Apr 9;177(1):7-11.

Cushing L, Kuang PP, Qian J, Shao F, Wu J, Little F, Thannickal VJ, Cardoso WV, Lü J., *miR-29 is a major regulator of genes associated with pulmonary fibrosis.,* Am J Respir Cell Mol Biol. 2011 Aug;45(2):287-94.

El-Andaloussi S, Lee Y, Lakhal-Littleton S, Li J, Seow Y, Gardiner C, Alvarez-Erviti L, Sargent IL, Wood MJ., *Exosome-mediated delivery of siRNA in vitro and in vivo.,* Nat Protoc. 2012 Dec;7(12):2112-26.

Eldh M, Lötvall J, Malmhäll C, Ekström K., *Importance of RNA isolation methods for analysis of exosomal RNA: evaluation of different methods.,* Mol Immunol. 2012 Apr;50(4):278-86.

Emily Zeringer, Mu Li, Tim Barta, Jeoffrey Schageman, Ketil Winther Pedersen, Axl Neurauter, Susan Magdaleno, Robert Setterquist and Alexander V Vlassov., *Methods for the extraction and RNA profiling of exosomes*, World J Methodol. 2013 March 26; 3(1): 11-18

Ernst O, Zor T., *Linearization of the bradford protein assay.*, J Vis Exp. 2010 Apr 12;(38).

Fan Y, Hsiung M, Cheng C, Tzanakakis ES., *Facile engineering of xeno-free microcarriers for the scalable cultivation of human pluripotent stem cells in stirred suspension*, Tissue Eng Part A. 2014 Feb;20(3-4):588-99.

Fernandes TG, Fernandes-Platzgummer AM, da Silva CL, Diogo MM, Cabral JM., *Kinetic and metabolic analysis of mouse embryonic stem cell expansion under serum-free conditions.*, Biotechnol Lett. 2010 Jan;32(1):171-9.

Frantz Christian, Stewart Kathleen M. and Weaver Valerie M., *The extracellular matrix at a glance* (2010), Journal of Cell Science 123, 4195-4200

Hinton A, Afrikanova I, Wilson M, King CC, Maurer B, Yeo GW, Hayek A, Pasquinelli AE., *A distinct microRNA signature for definitive endoderm derived from human embryonic stem cells.*, Stem Cells Dev. 2010 Jun;19(6):797-807

Horani A, Nath A, Wasserman MG, Huang T, Brody SL., *Rho-associated protein kinase inhibition enhances airway epithelial Basal-cell proliferation and lentivirus transduction*, Am J Respir Cell Mol Biol. 2013 Sep;49(3):341-7.

Hoveizi E, Nabiuni M, Parivar K, Ai J, Massumi M., (2013), *Definitive endoderm differentiation of human-induced pluripotent stem cells using signaling molecules and IDE1 in three-dimensional polymer scaffold.*, J Biomed Mater Res A., [Online], doi: 10.1002/jbm.a.35039

Hynes, R. O., *The extracellular matrix: not just pretty fibrils*, (2009) Science 326, 1216-1219

Jin S, Yao H, Weber JL, Melkoumian ZK, Ye K., *A synthetic, xeno-free peptide surface for expansion and directed differentiation of human induced pluripotent stem cells.*, PLoS One. 2012;7(11):e50880. doi: 10.1371/journal.pone.0050880. Epub 2012 Nov 30.

Kehoe DE, Jing D, Lock LT, Tzanakakis ES., *Scalable stirred-suspension bioreactor culture of human pluripotent stem cells*, Tissue Eng Part A. 2010 Feb;16(2):405-21

Kiichi Watanabe, Morio Ueno, Daisuke Kamiya, Ayaka Nishiyama, Michiru Matsumura, Takafumi Wataya, Jun B Takahashi, Satomi Nishikawa, Shin-ichi Nishikawa, Keiko Muguruma & Yoshiki Sasai, *A ROCK inhibitor permits survival of dissociated human embryonic stem cells*, Nature Biotechnology 25, 681 - 686 (2007)

Kim K, Doi A, Wen B, Ng K, Zhao R, Cahan P, Kim J, Aryee MJ, Ji H, Ehrlich LI, Yabuuchi A, Takeuchi A, Cunniff KC, Hongguang H, McKinney-Freeman S,Naveiras O, Yoon TJ, Irizarry RA, Jung N, Seita J, Hanna J, Murakami P, Jaenisch R, Weissleder R, Orkin SH, Weissman IL, Feinberg AP, Daley GQ., *Epigenetic memory in induced pluripotent stem cells*, Nature. 2010 Sep 16;467(7313):285-90

Krauss-Etschmann S, Bush A, Bellusci S, Brusselle GG, Dahlén SE, Dehmel S, Eickelberg O, Gibson G, Hylkema MN, Knaus P, Königshoff M, Lloyd CM,Macciarini P, Mailleux A, Marsland BJ, Postma DS, Roberts G, Samakovlis C, Stocks J, Vandesompele J, Wjst M, Holloway J., *Of flies, mice and men: a systematic approach to understanding the early life origins of chronic lung disease.,* (2012),Thorax. 2013 Apr;68(4):380-4

Larijani MR, Seifinejad A, Pournasr B, Hajihoseini V, Hassani SN, Totonchi M, Yousefi M, Shamsi F, Salekdeh GH, Baharvand H., *Long-term maintenance of undifferentiated human embryonic and induced pluripotent stem cells in suspension.,* Stem Cells Dev. 2011 Nov;20(11):1911-23

Lässer C, Eldh M, Lötvall J., *Isolation and characterization of RNA-containing exosomes.,* J Vis Exp. 2012 Jan 9;(59)

Li X., *MiR-375, a microRNA related to diabetes.,* Gene. 2014 Jan 1;533(1):1-4

Liang Y, Ridzon D, Wong L, Chen C., *Characterization of microRNA expression profiles in normal human tissues,* BMC Genomics. 2007 Jun 12;8:166.

Madonna R, Görbe A, Ferdinandy P, De Caterina R., *Glucose metabolism, hyperosmotic stress, and reprogramming of somatic cells.,* Mol Biotechnol. 2013 Oct;55(2):169-78

Mehdi Shafa, Brad Day, Akihiro Yamashita, Guoliang Meng, Shiying Liu, Roman Krawetz & Derrick E Rancourt, *Derivation of iPSCs in stirred suspension bioreactors,* Nature Methods 9, 465–466 (2012)

Nichols JE, Niles J, Riddle M, Vargas G, Schilagard T, Ma L, Edward K, La Francesca S, Sakamoto J, Vega S, Ogadegbe M, Mlcak R, Deyo D, Woodson L,McQuitty C, Lick S, Beckles D, Melo E, Cortiella J., *Production and assessment of decellularized pig and human lung scaffolds,* Tissue Eng Part A. 2013 Sep;19(17-18):2045-62

Olmer R, Lange A, Selzer S, Kasper C, Haverich A, Martin U, Zweigerdt R., *Suspension culture of human pluripotent stem cells in controlled, stirred bioreactors.,* Tissue Eng Part C Methods. 2012 Oct;18(10):772-84.

Olmer R, Singh H, Haverich A, Martin U., *Scalable expansion of human pluripotent stem cells in suspension culture,* Zweigerdt R, Nat Protoc. 2011 May;6(5):689-700

Peinado H, Alečković M, Lavotshkin S, Matei I, Costa-Silva B, Moreno-Bueno G, Hergueta-Redondo M, Williams C, García-Santos G, Ghajar C, Nitadori-Hoshino A, Hoffman C, Badal K, Garcia BA, Callahan MK, Yuan J, Martins VR, Skog J, Kaplan RN, Brady MS, Wolchok JD, Chapman PB, Kang Y, Bromberg J,Lyden D., *Melanoma exosomes educate bone marrow progenitor cells toward a pro-metastatic phenotype through MET.,* Nat Med. 2012 Jun;18(6):883-91

Podolska A, Anthon C, Bak M, Tommerup N, Skovgaard K, Heegaard PM, Gorodkin J, Cirera S, Fredholm M., *Profiling microRNAs in lung tissue from pigs infected with Actinobacillus pleuropneumoniae.,* BMC Genomics. 2012

Porciuncula A, Zapata N, Guruceaga E, Agirre X, Barajas M, Prosper F., *MicroRNA signatures of iPSCs and endoderm-derived tissues,* Gene Expr Patterns. 2013 Jan-Feb;13(1-2):12-20

Price AP, England KA, Matson AM, Blazar BR, Panoskaltsis-Mortari A., *Development of a decellularized lung bioreactor system for bioengineering the lung: the matrix reloaded,* Tissue Eng Part A. 2010 Aug;16(8):2581-91

Roccaro AM, Sacco A, Maiso P, Azab AK, Tai YT, Reagan M, Azab F, Flores LM, Campigotto F, Weller E, Anderson KC, Scadden DT, Ghobrial IM., *BM mesenchymal stromal cell-derived exosomes facilitate multiple myeloma progression.,* J Clin Invest. 2013 Apr 1;123(4):1542-55.

Rock J, Königshoff M., *Endogenous lung regeneration: potential and limitations,* Am J Respir Crit Care Med. 2012 Dec 15;186(12):1213-9

Russo Isabella, Bubacco Luigi, Greggio Elisa, *Exosomes-associated neurodegeneration and progression of Parkinson's disease,* Am J Neurodegener Dis 2012;1(3):217-225

Sana Mujahid, Tanya Logvinenko, MaryAnn V Volpe and Heber C Nielsen, *miRNA regulated pathways in late stage murine lung development, BMC* Developmental Biology 2013, 13:13

Sessa R, Hata A., *Role of microRNAs in lung development and pulmonary diseases.,* Pulm Circ. 2013 Apr;3(2):315-328.

Shafa M, Sjonnesen K, Yamashita A, Liu S, Michalak M, Kallos MS, Rancourt DE., *Expansion and long-term maintenance of induced pluripotent stem cells in stirred suspension bioreactors.,* J Tissue Eng Regen Med. 2012 Jun;6(6):462-72

Stoorvogel W., *Functional transfer of microRNA by exosomes,* (2012), Blood, vol. 119 no. 3 646-648

Takahashi K, Tanabe K, Ohnuki M, Narita M, Ichisaka T, Tomoda K, Yamanaka S., *Induction of pluripotent stem cells from adult human fibroblasts by defined factors,* Cell. 2007 Nov 30;131(5):861-72.

Tian Y, Zhang Y, Hurd L, Hannenhalli S, Liu F, Lu MM, Morrisey EE., *Regulation of lung endoderm progenitor cell behavior by miR302/367.,* Development. 2011 Apr;138(7):1235-45.

Tzong-Shi Lu, PhD., Szu-Yu Yiao, BS., Kenneth Lim, MD., Roderick V. Jensen, PhD., and Li-Li Hsiao, MD., Ph.D., *Interpretation of biological and mechanical variations between the Lowry versus Bradford method for protein quantification,* N Am J Med Sci. Jul 2010; 2(7): 325–328.

Valadi H, Ekström K, Bossios A, Sjöstrand M, Lee JJ, Lötvall JO. *Exosome-mediated transfer of mRNAs and microRNAs is a novel mechanism of genetic exchange between cells.,* Nat Cell Biol. 2007 Jun;9(6):654-9

Villa-Diaz LG, Ross AM, Lahann J, Krebsbach PH., *Concise review: The evolution of human pluripotent stem cell culture: from feeder cells to synthetic coatings.,* Stem Cells. 2013 Jan;31(1):1-7

Wahlgren J, De L Karlson T, Brisslert M, Vaziri Sani F, Telemo E, Sunnerhagen P, Valadi H, *Plasma exosomes can deliver exogenous short interfering RNA to monocytes and lymphocyte*, Nucleic Acids Res. 2012 Sep 1;40(17)

Wei R, Yang J, Liu GQ, Gao MJ, Hou WF, Zhang L, Gao HW, Liu Y, Chen GA, Hong TP., *Dynamic expression of microRNAs during the differentiation of human embryonic stem cells into insulin-producing cells,* Gene. 2013 Apr 15;518(2):246-55.

Xiao J1, Meng XM, Huang XR, Chung AC, Feng YL, Hui DS, Yu CM, Sung JJ, Lan HY., *miR-29 inhibits bleomycin-induced pulmonary fibrosis in mice.,* Mol Ther. 2012 Jun;20(6):1251-60

Yin M, Ren X, Zhang X, Luo Y, Wang G, Huang K, Feng S, Bao X, Huang , He X, Liang P, Wang Z, Tang H, He J, Zhang B, *Selective killing of lung cancer cells by miRNA-506 molecule through inhibiting NF-κB p65 to evoke reactive oxygen species generation and p53 activation,* (2014), Oncogene, p1-13

Yiren GU, Mingzhou LI, Kai ZHANG, Lei CHEN, An-an JIANG, Jinyong WANG, Xuebin LV and Xuewei LI, *Identification of suitable endogenous control microRNA genes in normal pig tissues,* Animal Science Journal (2011) 82, 722–728

Yu H, Jiang L, Sun C, Li Guo L, Lin M, Huang J, Zhu L., *Decreased circulating miR-375: a potential biomarker for patients with non-small-cell lung cancer.,* Gene. 2014 Jan 15;534(1):60-5.